Journal of Inflammation Research

Dovepress
Taylor & Francis Group

Open Access Full Text Article

ORIGINAL RESEARCH

Qimai Feiluoping Decoction Inhibits EndMT to Alleviate Pulmonary Fibrosis by Reducing PI3K/AKT/mTOR Pathway-Mediated the Restoration of Autophagy

Jing Ma[1,*], Lu Ding[1,*], Xiaoyu Zang[2,*], Yingying Yang[3], Wei Zhang[4], Xiangyan Li[1], Daqing Zhao[1], Zepeng Zhang[1], Zeyu Wang[1], Linhua Zhao[1], Xiaolin Tong[1]

[1]The Affiliated Hospital to Changchun University of Traditional Chinese Medicine, Changchun, Jilin, 130021, People's Republic of China; [2]College of Traditional Chinese Medicine, Changchun University of Chinese Medicine, Changchun, Jilin, 130117, People's Republic of China; [3]China-Japan Friendship Hospital, National Center for Integrated Traditional Chinese and Western Medicine, Beijing, 100029, People's Republic of China; [4]Gansu University of Chinese Medicine, Lanzhou, Gansu, 730000, People's Republic of China

*These authors contributed equally to this work

Correspondence: Xiaolin Tong, The Affiliated Hospital to Changchun University of Traditional Chinese Medicine, Changchun, Jilin, 130021, People's Republic of China, Email tongxiaolin66@126.com

---

Purpose: Pulmonary Fibrosis (PF) is a severe interstitial lung disease currently lacking effective prevention strategies. Endothelial mesenchymal transition (EndMT), a novel mechanism for fibroblast production, is closely associated with PF. The precise mechanisms underlying the contribution of EndMT-derived fibroblasts to PF, however, remain unclear.

Methods: Using network pharmacology, molecular docking, and molecular dynamics, we identified the key targets and pathways through which Qimai Feiluoping decoction (QM) combats PF. EndMT and autophagy proteins were quantified in bleomycin (BLM) - induced C57BL/6 mice, human umbilical vein endothelial cells (HUVECs), and zebrafish using Western blotting (WB), quantitative real-time polymerase chain reaction (qRT-PCR), immunohistochemistry (IHC), immunofluorescence (IF), Transwell migration assays, and transmission electron microscopy (TEM), revealing the targets and pathways through which QM mitigates PF.

Results: Network pharmacology, molecular docking, and molecular dynamics suggest that QM combats PF by modulating the PI3K/AKT/mTOR pathway. Observations from the study indicated that QM was found to alleviate EndMT by restoring autophagy, primarily through inhibition of the PI3K/AKT/mTOR signaling pathway in both BLM-induced C57 mice and HUVECs. Supporting evidence from zebrafish models demonstrated that QM not only counteracts EndMT but also improves a range of vascular functional disorders and remodeling issues following EndMT.

Conclusion: Our research validates the active compounds, core targets, and signaling pathways through which QM counters PF, providing valuable insights for its therapeutic application in PF management.

Keywords: Qimai Feiluoping decoction, pulmonary fibrosis, network pharmacology, molecular docking, endothelial mesenchymal transition, autophagy

---

Introduction

Pulmonary Fibrosis (PF) is a grave interstitial lung disease characterized by an elusive pathogenesis[1] and marked by high mortality and limited treatment options.[2] This condition is notably identified by lung tissue remodeling,[3] disrupted wound healing processes,[4] impaired gas exchange, and reduced in lung function,[5] culminating in symptoms such as cough and progressive breathing difficulties.[6] The adjusted incidence and prevalence of idiopathic pulmonary fibrosis (IPF) are estimated to be in the range of 0.09–1.30 and 0.33–4.51 per 10,000 persons, respectively. Both incidence and mortality climb with age and over time, and the median survival after diagnosis is only 3–5 years, placing IPF among the deadliest

Received: 27 January 2025
Accepted: 19 June 2025
Published: 26 June 2025

non-cancer lung diseases.[7,8] Recent data have indicated a significant rise in cases of fibrotic lung disease following coronavirus disease 2019 (COVID-19) infections,[9] with clinical reports showing marked radiological evidence of PF in patients recovering from severe COVID-19 cases.[10] The recognized anti-PF medications, Pirfenidone (PFD) and Nintedanib, have been shown to slow the decline in lung function by approximately 50%.[11,12] Although these medications enhance patient well-being and prolong life, they do not halt the disease's progression entirely.[13] Consequently, there is a pressing need for the development of novel therapeutic agents that can arrest or slow the progression of PF, offering improved treatment options beyond the current limitations of existing drugs.

The focus of PF research has primarily on alveolar epithelial cells, myofibroblasts, and inflammatory cells, with comparatively limited investigation into the role of endothelial cells (ECs) in PF pathogenesis. Nevertheless, recent studies have started to recognize the significance of EC dysfunction and vascular remodeling, particularly following the loss of pulmonary capillaries and the proliferation of bronchial perivascular endothelial cells in lung parenchyma, as pivotal in the progression of PF.[14] ECs are noted for their heterogeneity and adaptability, dynamically responding to various tissue demands in both physiological and pathological states. They constitute a crucial monolayer lining the inner walls of blood vessels, vital for maintaining vascular permeability and facilitating blood-tissue exchange.[15] In response to tissue injury or pathological stimuli, ECs could undergo EndMT, shedding endothelial characteristics and acquiring mesenchymal traits, such as increased mobility, invasiveness, and the expression of myofibroblast markers like α-SMA and Collagen I. This transformation is also characterized by a decrease in endothelial markers like VE-cadherin.[16] EndMT contributes to the disruption of the vascular barrier, heightened vascular permeability, and immune cell infiltration. Cytokines released by immune cells can further destabilize the vascular barrier and activate fibroblasts, intensifying PF.[17] Radiological studies in early-stage PF patients have revealed increased abnormal neovascular networks around fibrotic areas, but a reduced vascular distribution within the fibrotic lesions, compromising gas exchange, elevating pulmonary vascular resistance, and exacerbating PF.[18] Recent research has shown that in early Acute Respiratory Distress Syndrome (ARDS), pharmacological interventions can improve vascular dysfunction, inhibit EndMT, and mitigate post-ARDS PF development.[19] Moreover, in IPF patients and BLM-induced mouse lung fibrosis models, elevated levels of MMP19 protein not only exacerbated PF by promoting mononuclear cell infiltration in the alveoli but also facilitated EndMT in Human Pulmonary Microvascular Endothelial Cells (HPMECs) in vitro.[20] These findings collectively highlight the complex interplay between EndMT, vascular remodeling, and the pathophysiology of PF.

Current understanding of the molecular mechanisms that inhibit EndMT in PF is still developing. However, the link between autophagy and EndMT has been increasingly acknowledged. Autophagy, a cellular mechanism crucial for the turnover of intracellular materials, plays integral roles in various physiological and pathological settings, including defense, metabolism, and cellular quality control.[21] This process is essential for maintaining cellular homeostasis and stress resistance. Normally, autophagy helps remove harmful or unnecessary cellular components, where autophagosomes merge with lysosomes to form autolysosomes, ultimately recycling nutrients or materials back to the cell.[22] The fusion of autophagosomes with lysosomes, governed by the lipid components of autophagosomes, facilitates the expulsion of degraded products from the cell, aiding in their recycling.[23] In pathological conditions, autophagy serves as a defense mechanism against organelle damage and pathogen invasion, thereby preserving internal stability.[24] Recent studies have identified Irisin as a potential therapy that reduces perivascular fibrosis induced by doxorubicin in ECs through modulating reactive oxygen species (ROS) accumulation and autophagy disorder, consequently inhibiting EndMT.[25] Additionally, Plantamajoside (PMS), a natural compound derived from Plantago asiatica L., has been shown to impede the RAGE/autophagy/EndMT pathway activated by advanced glycation end products (AGEs), thus alleviating myocardial damage and functional disorders in congestive heart failure (CHF) mice, and demonstrating an anti-cardiac fibrosis effect.[26] These insights suggest that modulating autophagy in certain pathological states can inhibit EndMT, proposing that restoration of autophagy might be an effective strategy to counteract EndMT in PF.

Traditional Chinese medicine (TCM) attributes pulmonary fibrosis (PF) mainly to qi deficiency and blood stasis, a syndrome pattern common in PF patients. Qimai Feiluoping decoction (QM), a formula of 18 classic herbs listed in Table S1, replenishes qi, nourishes yin, promotes blood circulation, and opens the meridians, and it is widely used in TCM treatment of PF. Meanwhile, it has gained recognition for its role in the rehabilitation protocols for COVID-19 patients, officially endorsed by the National Health Commission of China (http://www.nhc.gov.cn/xcs/zhengcwj/202005/b15d59b5228341129cc8c5126f663b10.shtm). The efficacy of QM has been substantiated through a structured randomized controlled clinical trial (RCT) with the registration number ChiCTR2000032165. This study demonstrated significant alleviation of clinical symptoms such as cough, chest constriction, dyspnea, and fatigue in patients following a 24-week treatment period. Notably, improvements were observed in lung computed tomography (CT) findings, specifically in reducing ground-glass opacities, grid-like patterns, and fibrous strand shadows. Previous research has explored the pharmacological effects and mechanisms of QM on lung damage, establishing that QM can mitigate PF by influencing epithelial-mesenchymal transition (EMT), extracellular matrix (ECM) degradation, and the TGF-β signaling pathway.[27] Further studies utilizing BLM-induced C57 mice and TC-1 cell models have shown that QM can ameliorate PF conditions by reducing mitochondrial ROS content in lung tissues and cells, enhancing ATP production, and alleviating oxidative stress damage mediated by mitochondrial complex I.[28] With growing interest in ECs dysfunction and vascular remodeling in various diseases, and considering the significance of promoting blood circulation and removing blood stasis in QM therapy, this study focuses on exploring the targets and potential mechanisms through which QM addresses vascular injury-mediated PF.

Network pharmacology, an emerging field, integrates biological networks with drug action networks to explore the interrelationships between components and diseases. This methodology illuminates potential pathways through which TCMs may exert their effects, thereby enriching our understanding of their mechanisms in disease treatment. In contrast, molecular docking utilizes simulations of geometric structures and molecular interactions to inform drug design. Moreover, molecular dynamics simulations were conducted for 10 ns to estimate the ligand's stability within the protein under normal physiological conditions and to assist us in analyzing and studying the details of the interactions and stability between the selected ligands and the selected proteins. A 10 nanosecond molecular dynamics simulation assessed ligand stability within the protein under physiological conditions and clarified the specific ligand protein interactions.

Recently, the integration of the above technical methods have become a significant trend in drug research and discovery. Compared to standalone biological experiments, the efficacy of TCMs, when evaluated through network pharmacology combined with experimental validation, can be understood in a more comprehensive and objective manner. In our study, we utilized network pharmacology, molecular docking and molecular dynamics simulations to identify the core "disease-targets-pathways" through which QM mediates its anti-PF effects. Additionally, to further explore the efficacy and potential mechanisms of the natural product QM, experimental verification was conducted using BLM-induced C57 mice and HUVECs, along with zebrafish. The research flowchart is depicted in Figure 1.

Materials and Methods

Data Preparation

Collection of Targets of Main Active Compounds in QM and PF-Related Targets

Firstly, after oral administration of QM for 14 days, the mouse plasma (30 μL per mouse) and lung tissues (30 mg per mouse) from BLM group and BLM+QM group (n = 7) were collected to identify the possible active components of QM. The pre-cooled methanol was added into plasma or homogenized lung tissues to precipitate the protein, which was centrifuged at 13,000 rpm for 10 min for supernatant collection. Then, the supernatant was dried with nitrogen and dissolved with methanol for rapid characterization of the prototype compounds and their metabolites using a ACQUITY UPLC I-Class/Vion IMS-QTOF system (UHPLC/IM-QTOF-MS, Waters, Milford, United States). A C18 column (Acquity UPLC BEH, Waters) was used for chromatographic separation with optimal mobile phase. High-resolution MS data were recorded by MSE in both the positive and negative ESI mode, which was employed to identify prototype compounds and metabolites of QM using UNIFI™ 1.9.3.0 software (Waters). The key parameters were set as follows: the deviation range of the quality matching parameters was 20.00 ppm; metabolism groups included +H2, +O, +C2H2O, +SO3, and +C6H8O6. Secondly, we gathered target information based on active ingredient names and CAS numbers, followed by data processing. The primary databases utilized were TCMSP and TCMBank. Targets without prior information were predicted with the SEA tool (https://sea.bkslab.org) and retained only when the P value was $\leq 1.0 \times 10^{-15}$. Pulmonary fibrosis genes were then collected by searching "pulmonary fibrosis" in GeneCards (relevance score ≥ 10.0), DisGeNET, and OMIM, three databases widely trusted for disease related targets.

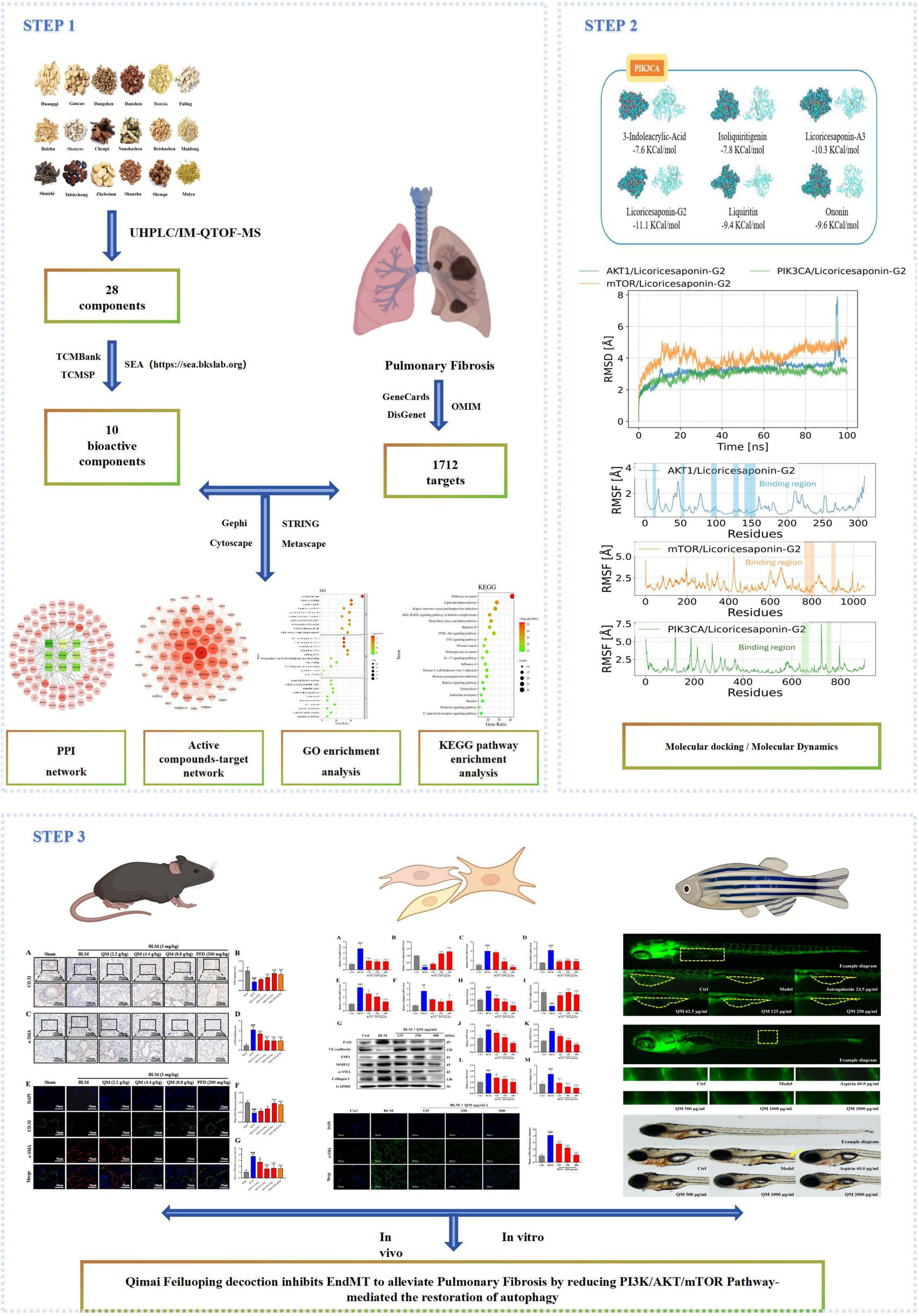

Figure 1 Process flowchart for research analysis.

Bioinformatics Analysis

Acquisition of Genes in the Intersection between QM and PF

To identify genes at the intersection between QM and PF, a Venn diagram was employed to visualize the overlapping regions among sets of elements. The principal target genes associated with both QM and PF were input into Venny 2.1 (http://bioinfogp.cnb.csic.es/tools/venny/). Using this tool, the intersecting targets of QM and PF were determined. This analysis successfully pinpointed potential target genes of QM relevant to the treatment of PF. Subsequently, the visualization software Cytoscape 3.7.2 was utilized to generate the compound-disease target network.

Protein–Protein Interaction Data

We established a protein–protein interaction (PPI) network using the STRING database (https://string-db.org/).[29] Initially, the overlapping targets of QM and PF were input into the STRING database to construct a preliminary PPI network diagram. The species was set to "Homo sapiens", with a combined score threshold of ≥ 0.40, and isolated nodes were removed. An enhanced PPI network diagram was then developed using Cytoscape software (version 3.7.2). Within Cytoscape, the "Network Analyzer" feature was employed to conduct an analysis using key metrics such as betweenness centrality (BC), closeness centrality (CC), and degree centrality (DC), which served as screening indices. These metrics were arranged in descending order. Following a comprehensive literature review, pivotal targets were identified.

GO and KEGG Pathway Enrichment

To delve into the signaling pathways and potential biological processes involved in the QM treatment of PF, we uploaded the intersecting targets of QM and PF to the Metascape database (https://metascape.org/gp/index.html). Within the "Functional Annotation" section, we selected cellular components (CC), molecular functions (MF), and biological processes (BP) under Gene Ontology (GO), along with the Kyoto Encyclopedia of Genes and Genomes (KEGG) pathways. After downloading the results, we refined them using Excel, setting parameters including Min Overlap=3, P value Cutoff=0.01, and Min Enrichment=1.5, prioritizing terms based on P-value. We visualized the top 20 KEGG pathway enrichment results in a bubble diagram and the top 10 GO enrichment results, based on gene number and P-value.

Molecular Docking

The preparation of macromolecule receptor files began with retrieving the crystal structure of the target protein from the Protein Data Bank (PDB) (http://www.rcsb.org/). The macromolecule receptor was then opened in PyMOL software to remove water molecules and ions. The cleaned protein receptor was subsequently saved as "PDBQT" files in AutoDockTools 1.5.6.

For the preparation of small molecule ligand files, the molecular structures of the compounds were sourced from the PubChem database (https://pubchem.ncbi.nlm.nih.gov/), and their 2D structures were imported into ChemBioDraw. These structures were then converted to 3D in AutoDockTools 1.5.6 and saved as "PDBQT" files for docking.

The construction of docking sites, docking, and visualization processes were carried out using AutoDockTools 1.5.6. The PDBQT structures of both receptors and ligands were imported to construct the docking sites. Molecular docking was performed using Vina software, which calculated the docking affinities. After the Vina simulation concluded, the docking calculations were reviewed. A default binding score of less than −5.0 kcal/mol indicates favorable binding activity between the ligand and receptor, while a score below −7.0 kcal/mol suggests a particularly strong binding affinity.[30]

Molecular Dynamics

Molecular dynamics simulations were performed using AMBER 22 software. Small molecule charges were calculated via the antechamber module and gaussian 09 software at HF/6-31G* level. GAFF2 and ff14SB force fields were used to describe small molecules and proteins, respectively.[31,32] Systems were prepared with LEaP module, solvated in TIP3P water boxes with 10Å distance, and neutralized with ions.

Energy minimization (2500 steps steepest descent followed by 2500 steps conjugate gradient) preceded 200 ps heating to 298.15 K, 500 ps NVT equilibration, 500 ps NPT equilibration, and a 100 ns NPT production run. A 10 Å cutoff was applied to nonbonded interactions, particle mesh Ewald treated long range electrostatics, SHAKE constrained hydrogen bonds, a Langevin thermostat ($\gamma = 2\ \mathrm{ps}^{-1}$) maintained temperature,[33,34] and pressure remained at 1 atm. The integration step was 2 fs, and trajectories were saved every 10 ps. MM/GBSA method was employed to calculate protein-ligand binding free energies using the last 10 ns trajectory data.[35,36] The binding energy was calculated as: ΔGbind = ΔGcomplex - (ΔGreceptor + ΔGligand) = ΔEinternal + ΔEVDW + ΔEelec + ΔGGB + ΔGSA. ΔGGB was calculated using the GB model (igb=2) developed by Nguyen et al, while ΔGSA was estimated as 0.0072 × ΔSASA.[37] Entropic contributions were omitted due to computational limitations.

Preparation of QM Powder Extract

In this study, a traditional water decoction method was utilized to extract the essence from various medicinal herbs, all sourced from the pharmacy at Changchun University of Traditional Chinese Medicine Affiliated Hospital in Changchun, China. The formulation consisted of the following herbs: Astragalus mongholicus Bunge (Huangqi) 15 g, Codonopsis pilosula Nannf (Dangshen) 9 g, Atractylodes macrocephala Koidz (Baizhu) 9 g, Adenophora triphylla (Thunb). A.DC (Nanshashen) 9 g, Glehnia littoralis F.Schmidt (Beishashen) 9 g, Ophiopogon japonicus (Thunb). Ker Gawl (Maidong) 15 g, Citrus aurantium L. (Chenpi) 9 g, Poria cocos (Schw). Wolf (Fuling) 15 g, Pinellia ternata (Thunb). Makino (Banxia) 6 g, Salvia miltiorrhiza Bunge (Danshen) 9 g, Fritillaria thunbergii Miq (Zhebeimu) 3 g, Whitmania pigra Whitman (Shuizhi) 3 g, Eupolyphaga sinensis Walker (Tubiechong) 3 g, Glycyrrhiza glabra L. (Gancao) 6 g, Crataegus pinnatifida Bunge (Shanzha) 3 g, Massa medicata fermentata (Shenqu) 3 g, Hordeum vulgare L. (Maiya) 3 g, and Dioscorea oppositifolia L. (Shanyao) 9 g. Plant names were verified using the World Flora Online database (https://www.worldfloraonline.org/). A total of 138 g of these herbs were soaked in distilled water for 2 hours, then boiled in 1380 mL of water (maintaining a 1:10 mass ratio) twice, each time for one hour. The resulting decoctions were combined and centrifuged at 8000 rpm for 15 minutes to separate the supernatant. This supernatant was then heated and concentrated to a viscous state, followed by vacuum dehydration and freeze-drying. The final product was 38 g of QM powder extract, representing a yield of 27.5%, and was stored at −80°C for future experimental use.

Reagents and Antibodies

BLM (HY17565) and pirfenidone (HYB0673) were obtained from MedChemExpress (Princeton, USA). Rapamycin (53123–88-9) was purchased from APExBIO Technology LLC (Houston, USA). VE-cadherin (BS70310), P-PI3K (BS4605), PI3K (BS9852M) and FSP1 (BS47554) were purchased from Bioworld (Nanjing, China). PAI1 (ab222754) was purchased from Abcam (Cambridge, USA). α-SMA (67735-1-Ig), Collagen I (14695-1-AP), CD31 (28,083-1-AP), MMP12 (22,989-1-AP), FSP1 (20,886-1-AP), P-AKT (66444-1-Ig), AKT (60203-2-Ig), mTOR (66888-1-Ig), P-mTOR (67778-1-Ig), LC3 (14,600-1-AP), Beclin-1 (11,306-1-AP), GAPDH (10494-1-AP) and goat anti-rabbit/mouse antibodies (SA00001-1, SA00001-2) were obtained from Proteintech (Wuhan, China).

Animal Experiment Design

The experimental protocol involving animals received approval from the Experimental Animal Ethics Committee of Changchun University of Chinese Medicine (Approval No. 2023589). Seventy 8-week-old male C57BL/6 mice were acquired from Beijing Vital River Laboratory Animal Technology Co., Ltd., Beijing, China. These mice were housed under optimal conditions (20 ± 2°C, 50–60% humidity) at the animal experiment center. PFD, a first-line drug for treating PF, was chosen as the positive control. Following a week-long acclimatization period, the mice were randomly divided into several groups: sham operation, BLM, QM (2.2, 4.4, 8.8 g/kg), and PFD (200 mg/kg), with each group comprising 10 mice. Before the experiments, all mice were anesthetized with an intraperitoneal injection of pentobarbital sodium (3 mL/kg). The sham operation group received an intra-tracheal injection of 0.9% saline (NS), while the other groups were administered BLM (3 mg/kg) following established protocols.[38] Starting the day after surgery, the mice received their respective treatments orally daily, with the sham and model groups receiving pure water. Two weeks after continuous medication, the mice underwent Quantum FX Micro CT scanning (PerkinElmer, Inc., Waltham, MA, USA), followed by euthanasia and sample collection for further analysis.

Cell Culture and Treatment

HUVECs were obtained from Wuhan Procell Life Science & Technology Co., Ltd., Wuhan, China. These cells were cultured in RPMI 1640 medium (Gibco, United States) supplemented with 10% Fetal Bovine Serum (FBS, Clark Bioscience, Claymont, United States), 100 kU/L penicillin, and 100 mg/L streptomycin (Biosharp, Hefei, China). For the study, HUVECs were divided into five groups: a normal group, a BLM group, and three groups treated with varying concentrations of a test substance (125, 250, and 500 μg/mL). The cells were incubated at 37°C in a humidified environment containing 5% CO_2. Once they reached 70–80% confluence, BLM (60 ng/mL) was administered to all groups except the normal group, and the co-culture was continued for 48 hours.

Zebrafish Experiment Design

The zebrafish experiments were conducted in collaboration with Hangzhou Hunter Biotechnology Co., Ltd., adhering to ethical guidelines under license SYXK (Zhe) 2012–0171 and complying with AAALAC international standards (Certification No.001458). Zebrafish were raised in water at 28°C for aquaculture. Water quality parameters included 200 mg of instant sea salt per 1 L of reverse osmosis water, with a conductivity of 450550 μS/cm, a pH range of 6.5~8.5, and hardness of 50~100 mg/L CaCO3. The experimental procedure was divided into two phases.

To evaluate the effectiveness of vascular regeneration, we utilized transgenic zebrafish, aged one day post-fertilization (1 dpf), marked with green fluorescent Fli-1 to trace the vascular lineage. Astragaloside IV (L2007265, sourced from Shanghai Aladdin Biochemical Technology Co., Ltd., Shanghai, China) was used as the reference compound. We randomly assigned 1 dpf zebrafish into various groups within a 6-well plate: a normal control, a model group (treated with simvastatin: U2DBF-IK, from Tokyo Chemical Industry Co., Ltd., Shanghai, China), and groups receiving different dosages of QM (62.5, 125, 250 μg/mL), as well as a group administered Astragaloside IV (23.5 μg/mL), each group containing 30 zebrafish. Except for the normal control, all groups were subjected to simvastatin treatment in water to induce a microvascular deficiency model in the zebrafish. After a 48 hours incubation at 28°C, five zebrafish from each group were randomly selected for imaging using a Nikon AZ100 electric focus continuous zoom fluorescence microscope. The data, focusing on the subintestinal vessel area, were analyzed using NIS-Elements D 3.20 advanced image processing software.

For the second phase of our study, focusing on the improvement of vascular endothelial injury, we utilized five-day post-fertilization (5 dpf) transgenic zebrafish with green fluorescent Fli-1 vascular lineage and wild-type AB lineage zebrafish. As a control, Aspirin (BJ54728, sourced from Bayer HealthCare Co., Ltd., Beijing, China) was used. We randomly assigned 5 dpf transgenic zebrafish into several groups within a 6-well plate: a normal control group, a model group (treated with Ponatinib: 13771, provided by MedChemExpress), groups receiving various concentrations of QM (500, 1000, 2000 μg/mL), and a group administered Aspirin (60 μg/mL), each consisting of 30 fish. Except for the normal control group, all other groups were treated with Ponatinib in water to induce an endothelial injury thrombosis model in the zebrafish. After an 18-hour incubation at 28°C, five zebrafish from each group were randomly selected for imaging under a fluorescence microscope to assess the diameter of the intersegmental blood vessels. Additionally, we employed 5 dpf wild-type AB lineage zebrafish and followed the same grouping and modeling protocols. After an 18-hour treatment at 28°C, these zebrafish were stained with toluidine blue (MKCC7501, Sigma, USA). Subsequently, five zebrafish from each group were randomly selected and imaged under an OLYMPUS SZX7 dissecting microscope, with the incidence rate of thrombosis in each group being calculated. Repeating the same procedures, after the 18-hour treatment period at 28°C, we selected five zebrafish from each group at random and recorded their blood flow videos using a heartbeat and blood flow analysis system (Zebralab3.3 (PB2084C), ViewPoint Life Sciences, France). The zebrafish blood flow velocity and cardiac output were analyzed using ZebraBlood 3.4 blood flow analysis software, evaluating the efficacy of QM in improving hemodynamics.

Micro-CT Imaging

To assess the extent of PF, five mice from each treatment group were anesthetized using isoflurane and positioned supine in the Quantum FX Micro CT scanner. Imaging parameters as are set followings: 90 kV tube voltage, 360° rotation, and 30 frames per second, and 6-min scan time, according to previous reports.[39]

Histopathology and Immunohistochemistry

The lung lobes were initially rinsed multiple times with chilled saline before fixation in 4% paraformaldehyde (Biosharp, Hefei, China). Subsequently, the lungs were embedded in paraffin and sectioned into 3 μm slices. These slices were stained with Hematoxylin & Eosin (H&E) and Masson's trichrome to facilitate detailed morphological examination. Observations for signs of inflammation and fibrosis were carried out using a Digital Microscope and Slide Scanner (M8, PreciPoint, Thuringia, Germany). Pathological scoring was conducted based on methodologies from previous studies.[40] For the assessment of EndMT and autophagy-related biomarkers in lung tissues, IHC staining was performed using antibodies against CD31, α-SMA, and LC3B. After dewaxing and antigen retrieval, tissue sections were incubated overnight at 4°C with these primary antibodies, followed by a 1 hour incubation with HRP-labeled secondary antibodies (Proteintech, IL, USA). Subsequently, DAB solution was applied to facilitate the development of brown staining. After a final counterstaining step with hematoxylin, the tissue sections were examined under magnification to select appropriate fields of view. For the quantitative analysis of these pathological findings, Image J software was utilized.

Immunofluorescence

Dewaxed lung tissue sections and treated HUVECs were incubated overnight with primary antibodies, including CD31, α-SMA, P-mTOR, and mTOR, at 4°C. This was followed by a one-hour incubation with corresponding secondary antibodies at room temperature. Nuclei were stained with DAPI (Solibol, Beijing, China) for 15 minutes. The samples were examined under a fluorescence microscope (Leica DMi8, Germany), and relevant fields were photographed. Quantitative analysis of the fluorescence expression was carried out using Image J software.

Quantitative Real-Time PCR Analysis

Total RNA was extracted from lung tissues and HUVECs using a total RNA extraction kit (Tiangen Biochemical Technology Co., Ltd., Beijing, China). Subsequently, 1 μg of total RNA was reverse transcribed into cDNA using an iScript cDNA synthesis kit (Tiangen Biochemical Technology Co., Ltd). qPCR analysis was conducted using the Bio-Rad CFX96 system. The expression levels of target genes were normalized using the $2^{-\Delta\Delta Ct}$ method with GAPDH as the reference gene. Primers, purchased from Sangon Biotech (Shanghai) Co., Ltd. (Shanghai, China), and their corresponding gene sequences are detailed in Table S2.

Western Blot Analysis

Proteins were extracted from lung tissues and HUVECs using pre-cooled RAPI lysis buffer, as previously described.[27] The protein concentration was determined using the BCA protein assay kit. Proteins were then separated by SDS-PAGE and transferred onto a PVDF membrane. The membrane was incubated overnight at 4°C with primary antibodies targeting VE-cadherin, PAI1, FSP1, MMP12, α-SMA, Collagen I, LC3B, Beclin-1, PI3K, phospho-PI3K (P-PI3K), AKT, phospho-AKT (P-AKT), mTOR, phospho-mTOR (P-mTOR), and GAPDH. After incubation with secondary antibodies for 1 hour at room temperature, protein bands were visualized using a chemiluminescence detection system. Quantitative analysis of protein expression was performed using Image J software.

CCK8 Assay for Cell Viability

HUVECs were seeded in a 96-well plate at densities of 3000, 5000, or 10000 cells per well. The cells were treated with QM at concentrations ranging from 7.8 to 1000 μg/mL for 24, 48, or 72 hours to assess the impact of QM on cell viability. Additionally, for co-treatment analysis with QM and Bleomycin (BLM), HUVECs were divided into control, model, and treatment groups. After the specified treatment durations, each well received 10 μL of CCK8 (MedChemExpress) and was incubated for 1 hour at 37°C in darkness. The absorbance at 450 nm was then measured using a spectrophotometer (American Bertten, SynergyMx).

Transwell Migration Assays

The migration of HUVECs was assessed using Transwell Boyden chambers from Corning Costar, Cambridge, USA, equipped with a polycarbonate filter with 8 μm pores. Cells were seeded into the upper chamber, which was pre-coated with Matrigel, and placed in a 24-well plate. The cells were incubated for 24 hours in a serum-free medium, treated with either BLM alone or in combination with QM. Following the incubation period, the medium in the upper chamber was discarded, and the cells were fixed with 4% paraformaldehyde for 2 hours. After fixation, the cells were washed with PBS to remove non-migrated cells from the upper surface of the membrane. Cells that migrated to the bottom surface of the membrane were stained with 5% Cresyl violet for 15 minutes. Photographs of the stained cells were then taken under a microscope for analysis.

Transmission Electron Microscopy

After centrifugation, the HUVECs pellet, roughly the size of a mung bean, was collected and fixed in electron microscopy fixative (G1102, Servicebio, Wuhan, China) at 4°C for 2–4 hours, with gentle resuspension. Subsequently, the sample was washed three times with 0.1 M phosphate buffer (pH 7.4), each wash lasting 3 minutes, and centrifugation was performed after each wash. The cell clumps were then embedded in pre-heated agarose. Following this, the sample was fixed in 1% osmium tetroxide (18456, Ted Pella Inc, Beijing, China) at room temperature for 2 hours in the dark. This step was succeeded by another three washes, each lasting 15 minutes. The sample then underwent a dehydration process using a series of alcohol solutions of increasing concentrations, followed by infiltration and embedding in resin (90529–77-4, SPI, Tianjin, China). The resin block was subsequently cured in an oven at 60°C for 48 hours before removal. Ultrathin sections of 60–80 nm were prepared and stained with 2% uranyl acetate saturated alcohol solution in the dark for 8 minutes, followed by three washes with 70% alcohol and ultra-pure water. Further staining was conducted with a 2.6% lead citrate solution for 8 minutes, avoiding CO2 exposure. This was followed by three additional washes with ultra-pure water and gentle drying with filter paper. The sections were left to dry overnight at room temperature. Finally, the samples were examined and images were captured using a transmission electron microscope (HT7800/HT7700, HITACHI, Japan).

Statistical Analysis

Experimental results were presented as mean ± standard deviation, based on data from at least three independent experiments. Data analysis was performed using GraphPad Prism version 9.0. To determine statistical significance among multiple groups, one-way ANOVA followed by Tukey's post hoc test was employed. A p-value of less than 0.05 was considered to indicate statistical significance in all the statistical tests conducted.

Results

Main Active Molecules and Target Acquisition

In mouse plasma and lung tissues treated with QM, we identified a total of 28 components (Table S3). Using the TCMSP and TCMBank databases, along with the SEA tool for predicting targets for components lacking known target information, we removed duplicate values and converted protein names into gene symbols, resulting in 10 active ingredients and 293 targets (Table S4). Additionally, 1712 PF-related targets were identified from three databases: 712 from GeneCards (Relevance score ≥ 10.0), 924 from DisGeNET, and 76 from OMIM (Table S5). Subsequently, by employing VENN analysis, we determined 80 common targets between QM and PF, and identified 9 common active compounds for further study (Figure 2A)(Table S6).

Active Ingredient-Target Network

To further elucidate the relationship between the 9 active compounds and the 80 cross target genes at the system level, we constructed an active ingredient-target network using Cytoscape 3.7.2 (Figure 2B). In the network diagram, the red circles represent the common targets of QM and PF. The green rectangles represent the active ingredients, visually distinguishing them from the targets and emphasizing their role as key modulators within this network.

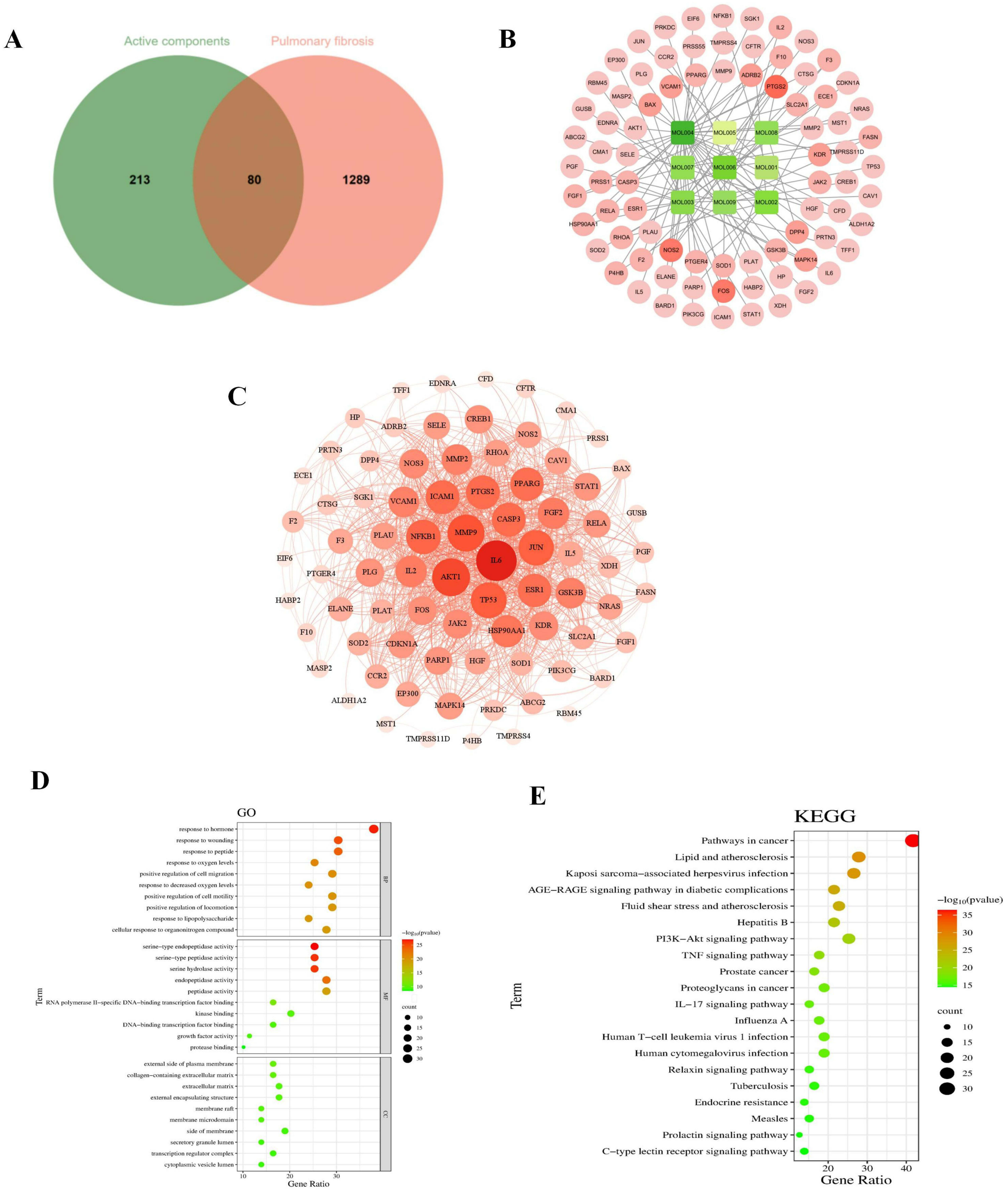

Figure 2 Target selection and network construction. (**A**) Venn diagram depicting potential targets for PF treatment with QM. (**B**) The "drug-active compounds-target network". The red circle represents common targets of QM and PF, and the green circle represents common active compounds. (**C**) PPI network of QM-targeted common proteins for PF therapy, with darker hues suggesting greater relevance. (**D**) GO enrichment analysis. (**E**) KEGG pathway enrichment analysis.

PPI Network Construction and Analysis

Utilizing the STRING database, we uploaded the intersecting targets and specified Homo sapiens as the species to generate a PPI network. We set the combined-score threshold to ≥ 0.40 and excluded disconnected nodes. The resulting PPI network data, in TSV format, was then downloaded and imported into Cytoscape 3.7.2 for visualization, resulting in a refined network as illustrated in (Figure 2C). This network comprised 79 nodes and 905 edges. In the visual representation, node size and color intensity are based on degree values, with larger and darker nodes indicating higher degrees. This visualization strategy helps to emphasize nodes with significant connectivity and potential importance in the network. Edge color intensity is set based on the relationship value score between target points, with darker edges indicating stronger interactions. This feature helps to highlight the most significant interactions within the network. The analysis identified the top five target nodes as IL6 (degree=63), AKT1 (degree=56), MMP9 (degree=54), TP53 (degree=51), and JUN (degree=50). These targets likely play crucial roles in the anti-PF effects of QM.

GO Function and KEGG Pathway Enrichment Analysis

In the study, the 79 targets identified in the PPI network were submitted to Metascape software to conduct GO and KEGG enrichment analysis. A total of 1237 statistically significant GO terms were retrieved, including 1102 related to BP, 85 to MF, and 50 to CC (Table S7). The top 10 significant enrichment terms of BP, MF, and CC with the highest gene counts were displayed in a bubble diagram. Among the BP categories, significant terms were predominantly associated with responses such as "response to wounding", "response to oxygen levels", "positive regulation of cell migration", and "positive regulation of cell motility", For the CC category, terms were primarily linked to "external side of plasma membrane", "collagen-containing extracellular matrix", "extracellular matrix", and "external encapsulating structure". In terms of MF, the main associations were with "serine-type endopeptidase activity", "serine-type peptidase activity", "serine-type hydrolase activity", and "endopeptidase activity". These findings are visually represented in Figure 2D. The KEGG pathway analysis revealed 156 pathways associated with PF, with the top 20 significant enrichment terms displayed in a bubble diagram (Figure 2E). Notable pathways include the "AGE-RAGE signaling pathway", "PI3K-Akt signaling pathway", "TNF signaling pathway", and "IL-17 signaling pathway". These results indicate that QM plays a critical role in the treatment of PF through its interaction with multiple targets and pathways. Notably, the PI3K/AKT/mTOR pathway, an autophagy regulator, controls the initiation and progression of pulmonary fibrosis; its inhibition dampens inflammation, curbs cell migration, and reduces extracellular matrix deposition, thereby slowing disease advancement.

QM Reduces EndMT in BLM-Induced C57 Mice and HUVECs

To accurately replicate the PF disease model, we utilized the established method of mouse tracheal instillation, a technique foundational to our previous research efforts.[39] This method has been instrumental in pathologically validating the PF model. To ensure the validity of our baseline models for subsequent experiments, we performed additional validations using Micro CT, H&E, and Masson's trichrome staining (Figure S1A–E). Hematoxylin–eosin staining showed pronounced histopathological alterations in lungs from BLM-treated mice (Figure S1C). Relative to sham controls, these lungs exhibited extensive connective-tissue proliferation (black arrows), blurred alveolar architecture, and widespread lymphocyte and neutrophil infiltration (yellow arrows). Additional features included dense perivascular inflammatory cuffs (red arrows), cytoplasmic vacuolization of bronchial epithelial cells (blue arrows), numerous enlarged alveolar spaces (green arrows), and abundant macrophages with eosinophilic cytoplasm within the airspaces (brown arrows). Treatment with QM or PFD markedly attenuated both inflammatory and fibrotic lesions. Masson's trichrome staining (Figure S1D) further confirmed these effects: the BLM group showed substantial collagen deposition (blue), which significantly decreased after treatment, as quantified in Figure S1E. Overall, QM markedly reduces BLM-induced pulmonary inflammation, collagen accumulation, and structural damage. These validations provided critical confirmation that informed our subsequent experimental endeavors.

Our study focused on exploring the role of EndMT in the formation of PF, particularly examining the regulatory effects of QM in BLM-induced PF in mice. Key proteins for detecting EndMT, the endothelial marker CD31, and the mesenchymal marker α-SMA, were analyzed. IHC and IF were used to assess the levels of CD31 and α-SMA proteins in lung tissues. In the BLM-induced mice, we observed an increase in α-SMA expression and a decrease in CD31.

However, following treatment with QM or PFD, α-SMA levels significantly decreased while CD31 levels showed an upward trend (Figure 3A–G).To delve deeper into QM's inhibitory impact on EndMT at the molecular level, qPCR and WB analyses were employed. Compared to the sham group, the BLM group exhibited reduced VE-cadherin mRNA expression and increased mRNA levels of PAI1, FSP1, MMP12, α-SMA, and Collagen I. Post-treatment, there was an upregulation of VE-cadherin mRNA and a decrease in the expression of other markers (Figures 4A–F). These findings were corroborated by WB results (Figures 4G–M).

Additionally, we investigated BLM-induced changes in HUVECs in vitro, determining appropriate dosages for QM and BLM based on existing literature[41] and the CCK8 method. The experiments employed concentrations of QM (125, 250, 500 µg/mL) and BLM (60 ng/mL) (Figure S2A–F). Morphological assessments revealed that BLM-treated HUVECs became elongated and spindle-shaped, while QM treatment led to slight morphological improvements (Figure S3A). Transwell assays demonstrated enhanced migration in BLM-modeled HUVECs, which was inhibited by QM (Figure S3B and C). At the gene and protein expression levels, BLM-treated cells displayed a loss of endothelial characteristics and an increase in mesenchymal markers, indicative of BLM-induced EndMT. QM treatment effectively inhibited these changes in protein expression (Figure 5A–M). IF analysis of α-SMA protein showed increased fluorescence in BLM-induced HUVECs, which was normalized following QM treatment (Figure 5N and O). Collectively, these results suggest that QM effectively mitigates EndMT and restores the expression of fibrosis markers in both in vivo and in vitro BLM-induced models.

QM Restores Autophagy in BLM-Induced C57 Mice and HUVECs

Autophagy, under certain pathological conditions, can ameliorate EndMT. Beclin-1 and LC3B are critical molecular markers in the autophagic process.[42] During autophagy, microtubule-associated protein 1A/1B-light chain 3 (LC3) is hydrolyzed to form LC3-I, which then converts to LC3-II through phosphatidylethanolamine (PE) conjugation. This conversion is essential for autophagosome formation, as LC3-II selectively binds to autophagosome membranes. Beclin-1, essential to the autophagic pathway, plays a pivotal role in autophagosome formation, extension, and maturation. In our study, the expression levels of Beclin-1 and LC3B II/I were diminished in the BLM group compared to the sham group. However, treatments with QM or PFD significantly restored these levels (Figure 6A–C). IHC testing of LC3B corroborated this finding, with the BLM group exhibiting reduced LC3B positive expression in lung tissue, which was significantly ameliorated following QM or PFD treatment (Figure 6D and E).

Further experiments on HUVECs induced by BLM verified QM's effects on autophagy. WB results indicated that Beclin-1 and LC3B II/I expression decreased in the model group compared to the control, but QM treatment restored their levels (Figure 6F–H). To further assess autophagic activity, TEM was employed to examine the ultrastructure of HUVECs. In the control group, most mitochondria (M) were structurally intact, the rough endoplasmic reticulum (RER) appeared normal, and numerous autophagic lysosomes (ASS) were observed. In contrast, the model group displayed swollen mitochondria, expanded RER, and a lack of typical autophagic structures. Treatment with QM ameliorated these issues, reducing mitochondrial swelling and significantly increasing the presence of autophagic lysosomes (Figure 6I). These findings suggest that QM alleviates EndMT by restoring autophagy.

QM Exerts Lung Protective Effects by Inhibiting the PI3K/AKT/mTOR Signaling Pathway

Having established the significant roles of EndMT and autophagy in the pathogenesis of PF, we further explored their internal mechanisms of action. Prior network pharmacology studies have indicated a close association between the development of PF and the PI3K/AKT signaling pathway.[27] The mTOR signaling cascade, known for its critical role in regulating autophagy, is primarily modulated through mTOR activity.[43] In our study, both PCR and WB analyses on BLM-induced mouse lung tissues and HUVECs revealed that QM treatment significantly reduced the expression of phosphorylated proteins (Figures 7–8). To further confirm the involvement of the mTOR pathway in EndMT in BLM-induced HUVECs, we introduced the specific mTOR inhibitor, rapamycin, for experimental validation. The cells were categorized into several groups: control, BLM, BLM +QM (500 µg/mL), BLM+rapamycin (100 nM),[41] and BLM+QM+rapamycin. WB results demonstrated that rapamycin considerably reduced the phosphorylation of the mTOR protein in BLM-induced HUVECs. Notably, the simultaneous use of

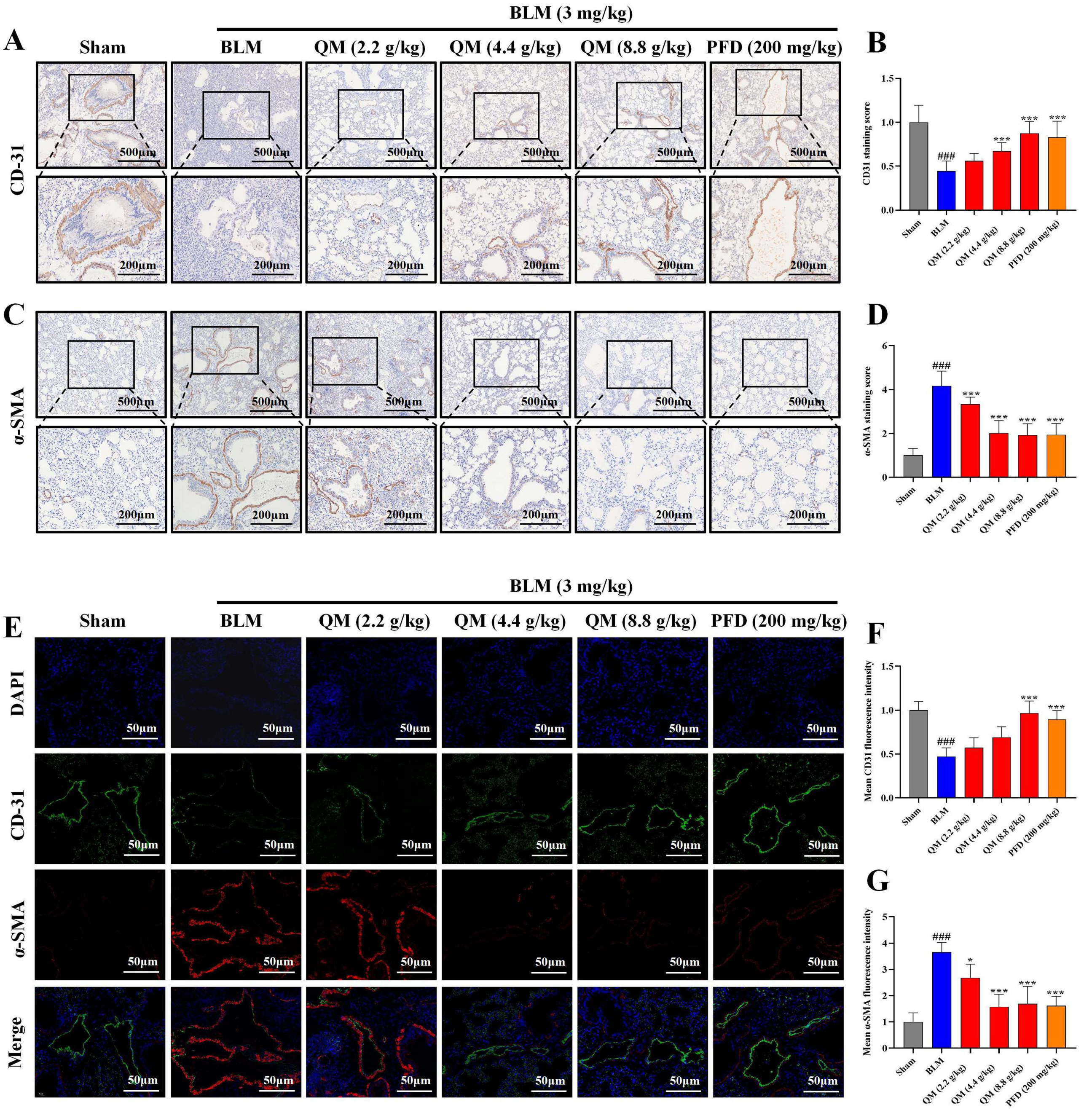

Figure 3 QM's mitigation of EndMT in C57 Mice: IHC and IF analysis. (**A**) IHC image of CD31. (**B**) CD31 protein expression quantification. (**C**) IHC image of α-SMA. (**D**) α-SMA protein expression quantification (Lower panel images, scale bar = 200 μm, are zoomed-in versions from upper panel, scale bar = 500 μm). (**E**) IF image of CD31 and α-SMA (Scale bar = 50 μm). (**F** and **G**) Quantitative analysis of CD31 and α-SMA protein expressions. (n = 5). $^{*}p < 0.05$, $^{***}p < 0.001$, compared to the BLM group. $^{\#\#\#}$ $p < 0.001$, compared to the Sham group.

rapamycin and QM further decreased the phosphorylation levels (Figure 9A and B). IF results corroborated these findings (Figure 9C–E). Meanwhile, in order to investigate the impact of autophagy activators (rapamycin) on EndMT, we added assays for PAI1, VE-cadherin, Collagen I, MMP12, α-SMA, and FSP1 under rapamycin. qPCR and WB results demonstrated that rapamycin considerably reduced the expression of the PAI1, Collagen I, MMP12, α-SMA, and FSP1 protein level in BLM-induced HUVECs, and improved the VE-cadherin expression. Notably, the simultaneous use of rapamycin and QM further decreased the expression levels (Figure 10A–M). These results confirm that QM exerts protective effects on the lungs by inhibiting the PI3K/AKT/mTOR signaling pathway, restoring autophagy, and mitigating EndMT.

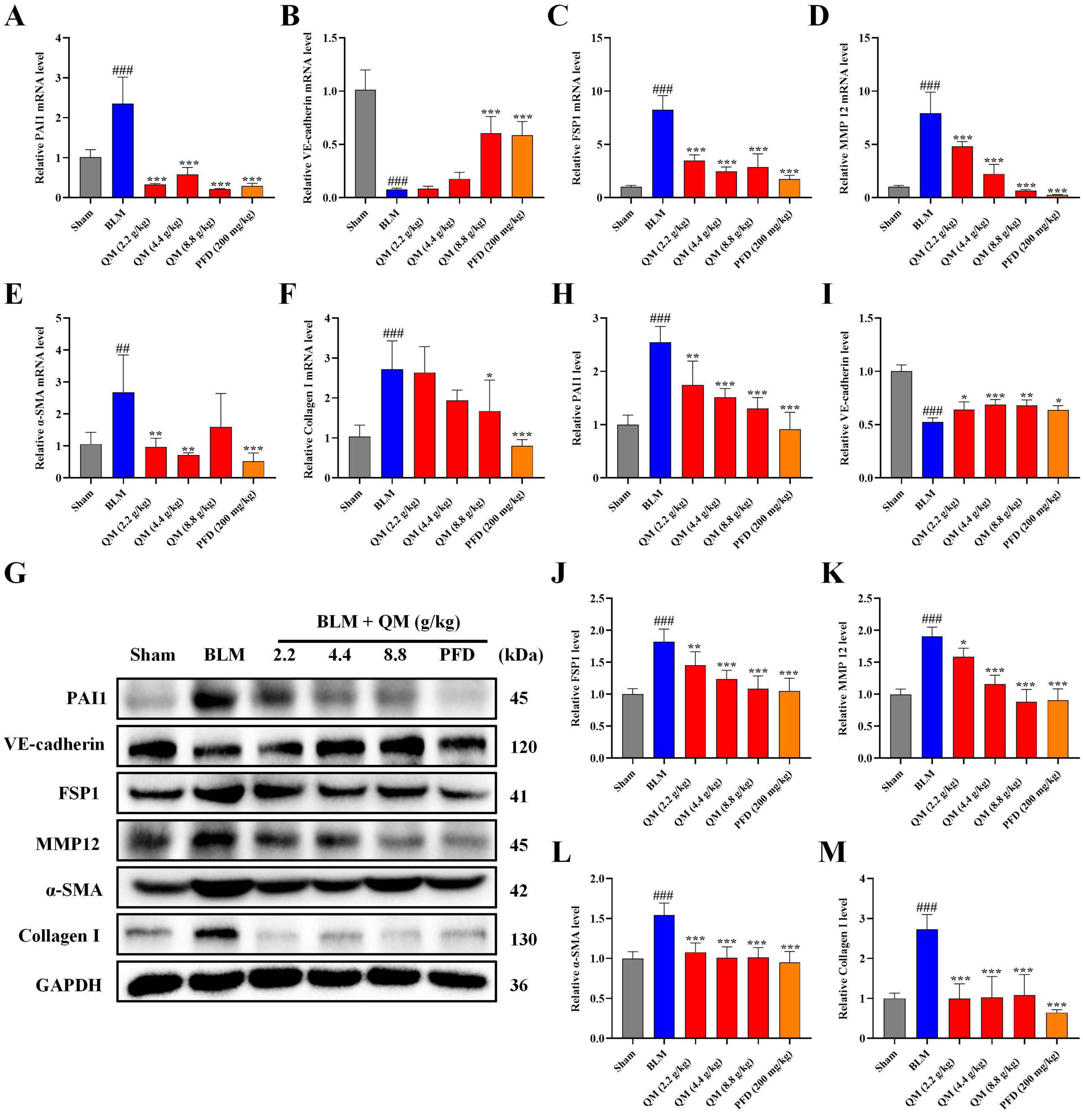

Figure 4 Assessment of QM's effect on EndMT in C57 mice using qPCR and WB techniques. (**A**–**F**) qPCR results for mRNA levels of PAI, VE-cadherin, FSP1, MMP12, α-SMA, and Collagen I in lung tissue. (**G**) WB analysis for protein expression of these markers. (**H**–**M**) Quantitative evaluation of protein levels using Image J software (n = 5). $^{*}p < 0.05$, $^{**}p < 0.005$, $^{***}p < 0.001$, compared to the BLM group. $^{\#\#}$ $p < 0.005$, $^{\#\#\#}$ $p < 0.001$, compared to the Sham group.

Molecular Docking and Molecular Dynamics Simulation

We further investigated the relationship between six effective compounds detected in blood and lung tissue and their interaction with the PI3K/AKT/mTOR signaling pathway. The molecular docking method was employed to analyze the binding energy with PIK3CA, AKT1, and mTOR (Figure 11). The results revealed that all six compounds have good binding ability with PIK3CA, AKT1, and mTOR, indicating that these compounds from QM may potentially inhibit the progression of PF by regulating the PI3K/AKT/mTOR signaling pathway.

Figure 12 summarizes the 100 ns molecular dynamics simulations of Licoricesaponin G2 bound to AKT1, mTOR, and PIK3CA. Global stability: The root mean square deviation (RMSD) for the AKT1 complex climbed quickly to 3.5 Å and later

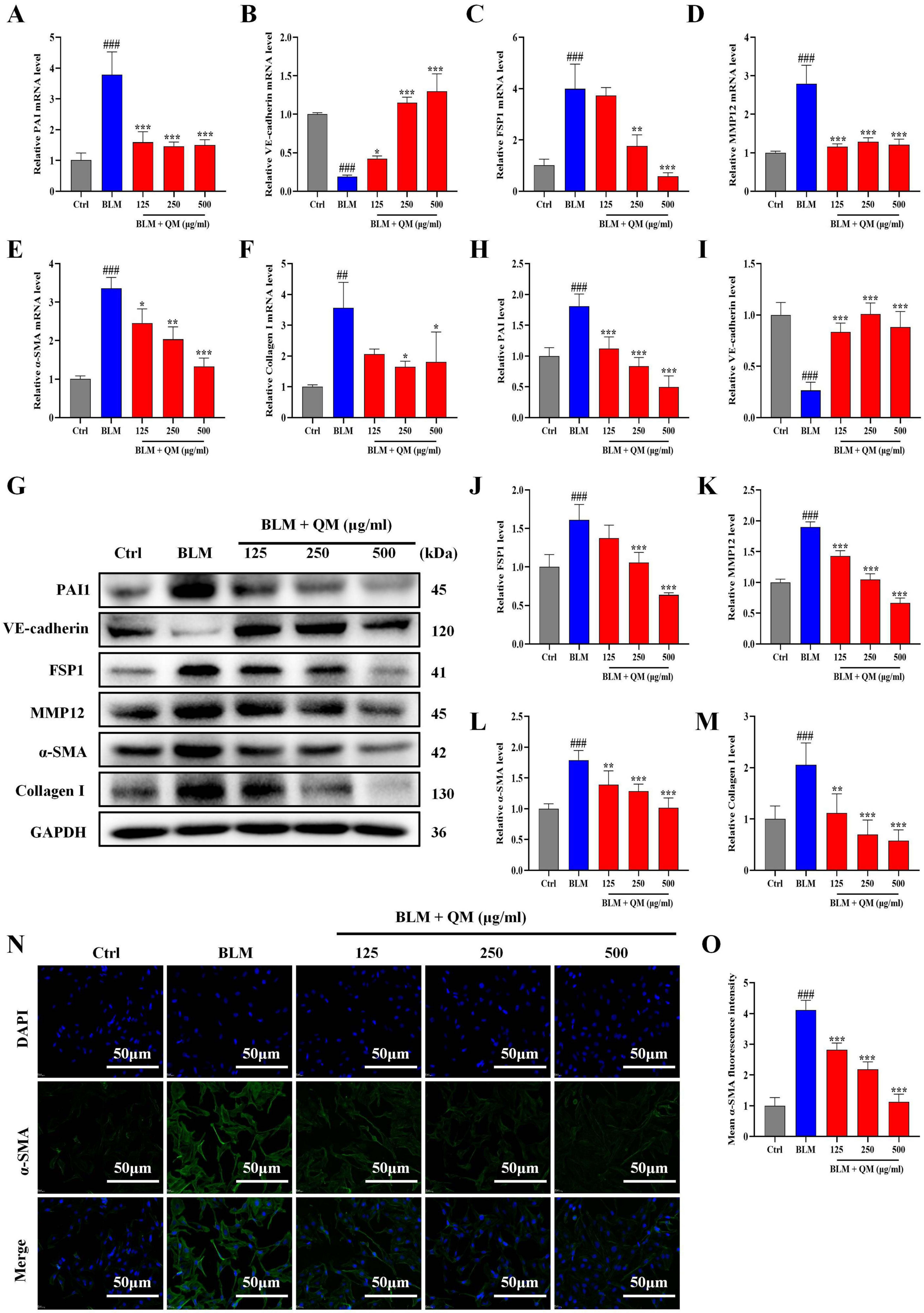

Figure 5 Evaluation of QM's effect on EndMT in HUVECs via qPCR, WB, and IF techniques. (**A**–**F**) qPCR analysis for mRNA expression levels of PAI, VE-cadherin, FSP1, MMP12, α-SMA, and Collagen I in HUVECs. (**G**) WB investigation of these proteins' expression in HUVECs. (**H**–**M**) Image J software quantification of protein expression. (**N**) IF image showcasing α-SMA (Scale bar = 50 μm). (**O**) Quantitative assessment of α-SMA protein expression (n ≥ 3). *p < 0.05, **p < 0.005, ***p < 0.001, compared to the BLM group. $^{\#\#}$ p < 0.005, $^{\#\#\#}$ p < 0.001, compared to the Ctrl group.

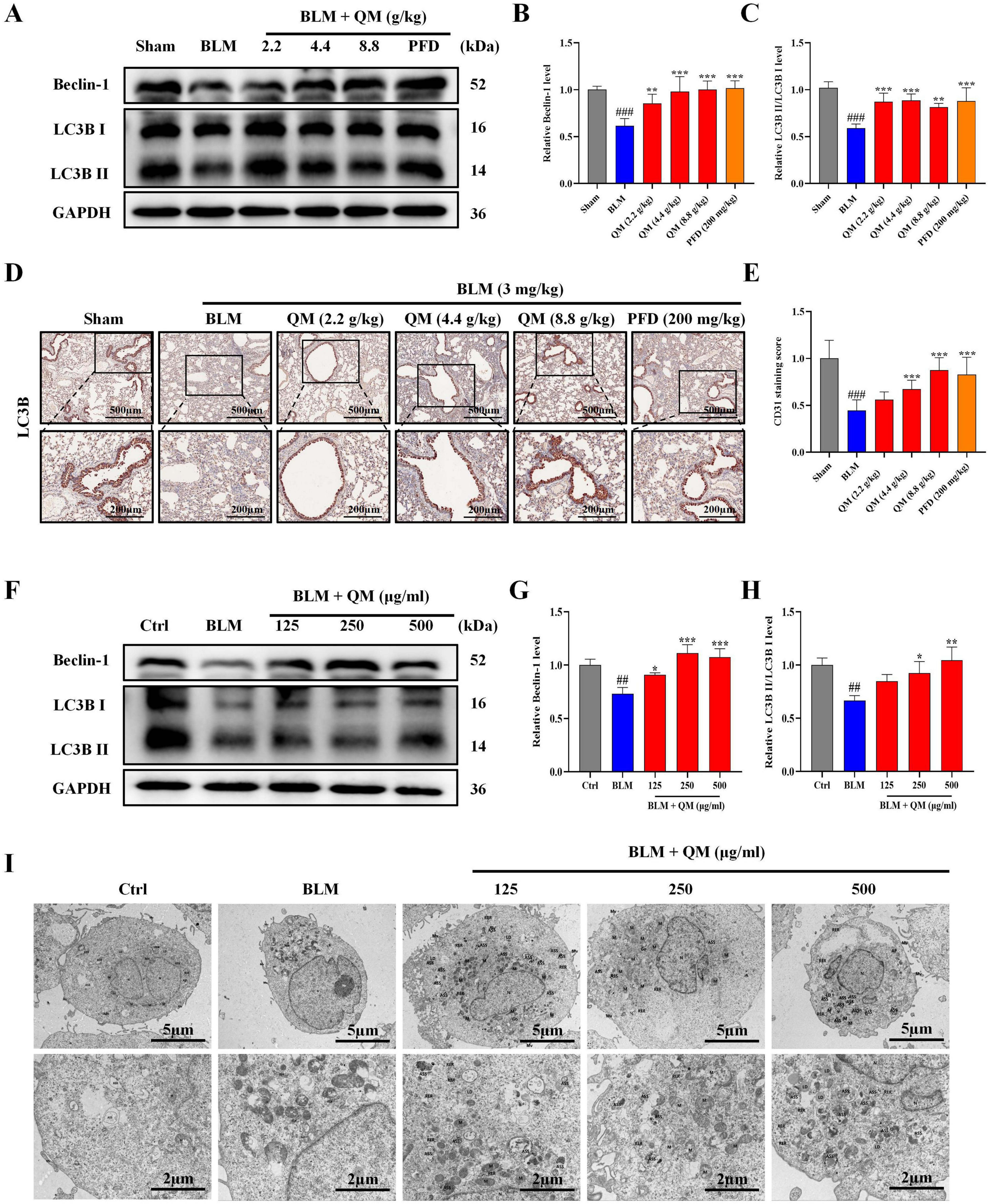

Figure 6 Assessment of QM's role in restoring autophagy in C57 mice and HUVECs: WB, IHC, and Electron Microscopy. (**A**) WB analysis of Beclin-1 and LC3B proteins in mouse lung tissue. (**B** and **C**) Quantitative protein expression evaluation via Image J software. (**D**) IHC image showing LC3B distribution. (**E**) Quantitative LC3B expression analysis (Lower panel images, scale bar = 200 μm, enlarged from upper panel insets, scale bar = 500 μm) (n = 5). $^{*}p < 0.05$, $^{**}p < 0.005$, $^{***}p < 0.001$, compared to BLM group. $^{\#}$ $p < 0.05$, $^{\#\#}$ $p < 0.005$, $^{\#\#\#}$ $p < 0.001$, compared to Sham group. (**F**) WB detection of Beclin-1 and LC3B protein expression in HUVECs. (**G** and **H**) Quantitative protein expression evaluation via Image J software. (**I**) TEM images of HUVECs. N nucleus; M mitochondria; (Images in the lower panel (scale bar = 2 μm) are magnified from the microphoto insets in the upper panel (scale bar = 5 μm)). (n ≥ 3). $^{*}p < 0.05$, $^{**}p < 0.005$, $^{***}p < 0.001$, compared to the BLM group. $^{\#\#}$ $p < 0.005$, $^{\#\#\#}$ $p < 0.001$, compared to the Ctrl group.

Abbreviations: ASS, autolysosome; AP, autophagosome; RER, rough endoplasmic reticulum; Go: Golgi apparatus; LD, lipid droplet; Mv, microvilli; Nu, nucleolus.

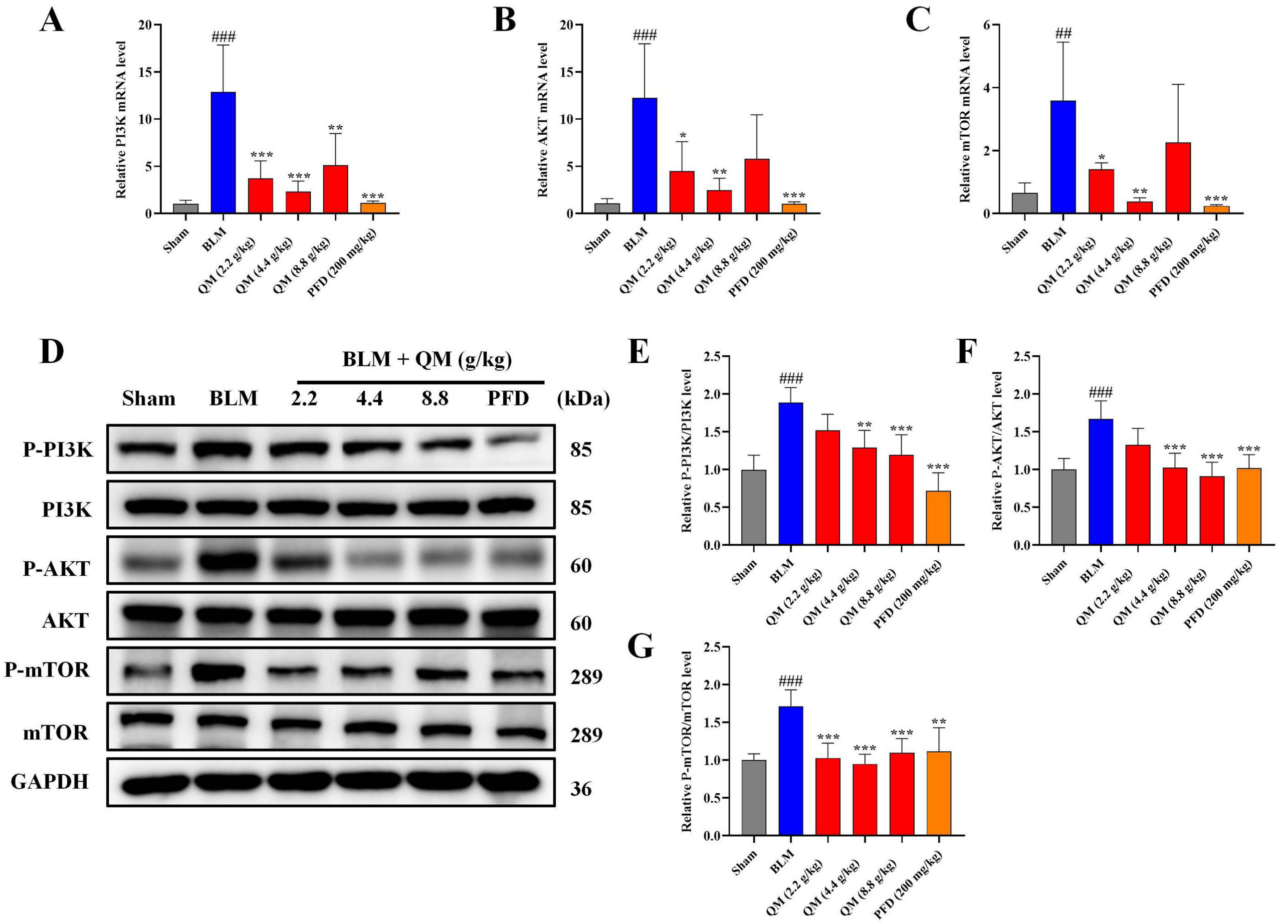

Figure 7 QM's inhibition of PI3K/AKT/mTOR pathway phosphorylation in C57 mice: qPCR and WB analysis. (**A**–**C**) qPCR detection of mRNA expressions in PI3K, AKT, and mTOR of the mouse lung tissue. (**D**) WB detection of protein expressions in P-PI3K, PI3K, P-AKT, AKT, P-mTOR, and mTOR of the mouse lung tissue. (**E**–**G**) Quantitative analysis of protein expressions using Image J software. (n = 5). *p < 0.05, **p < 0.005, ***p < 0.001, compared to the BLM group. $^{\#\#}$ p < 0.005, $^{\#\#\#\#}$ p < 0.001, compared to the Sham group.

exceeded 6 Å, indicating poor stability (Figure 12A). The mTOR complex held an RMSD of 4.0–5.5 Å, reflecting moderate stability, whereas the PIK3CA complex stayed below 3.0 Å with minimal fluctuation, signifying the most stable binding mode. Local flexibility: Root mean square fluctuation (RMSF) values were low across most residues except the termini; the binding loops were especially rigid, supporting stable ligand association (Figure 12B). Compactness: Radius of gyration (Rg) remained steady throughout (Figure 12C): ~20 Å for AKT1 (slightly increasing), ~30 Å for PIK3CA, and >35 Å for mTOR, confirming an absence of large scale conformational changes. Binding affinity: MM GBSA calculations from the final 10 ns produced binding free energies of 18.35 ± 5.13 kcal mol^{-1} for AKT1, –26.61 ± 3.89 kcal mol^{-1} for mTOR, and –30.24 ± 3.67 kcal mol^{-1} for PIK3CA (Figure 12D). Van der Waals and electrostatic terms dominated the favorable contributions, whereas solvation opposed binding. Thus, PIK3CA exhibited the strongest affinity. Hydrogen bonding: The AKT1 complex showed an unstable hydrogen bond network that weakened late in the trajectory (Figure 12E). The mTOR complex consistently maintained about five hydrogen bonds, whereas the PIK3CA complex stabilized at two to three bonds after 25 ns. These bonding patterns align with the stability and energy profiles observed for each complex.

QM Promotes Vascular Regeneration in Zebrafish and Exerts Protective Effects on Vascular Endothelial Cell Damage

Previous studies have established that EndMT is a critical step affecting endothelial dysfunction and vascular remodeling. Our experiments further demonstrated that QM can alleviate EndMT by restoring autophagy. Building on this foundation,

https://doi.org/10.2147/JIR.S515286

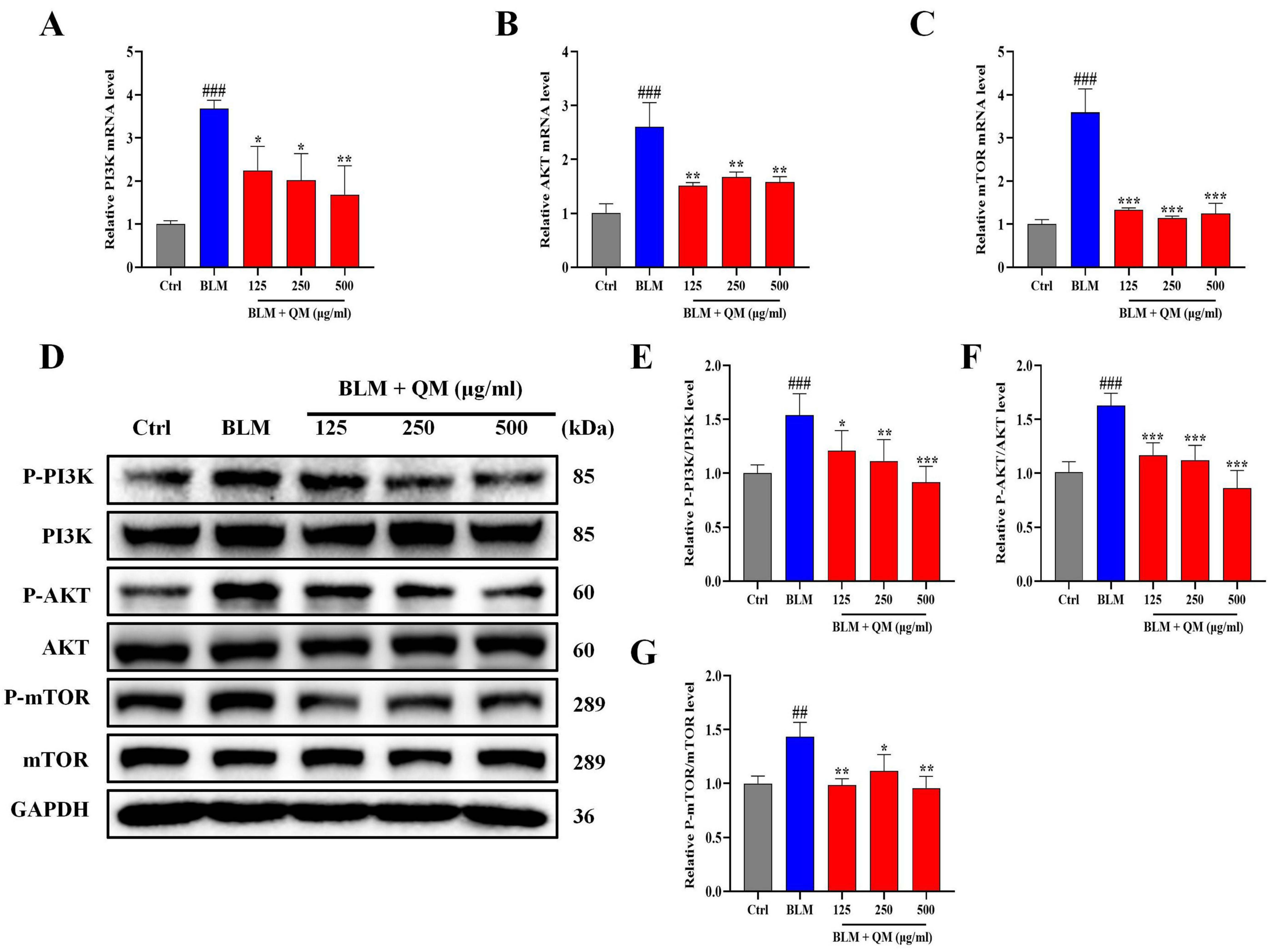

Figure 8 QM's inhibition of PI3K/AKT/mTOR pathway in HUVECs: qPCR and WB methods. (**A**–**C**) qPCR detection of mRNA expressions in PI3K, AKT, and mTOR in HUVECs. (**D**) WB detection of protein expressions of P-PI3K, PI3K, P-AKT, AKT, P-mTOR, and mTOR in HUVECs. (**E**–**G**) Quantitative analysis of protein expressions using Image J software. (n ≥ 3). *p < 0.05, **p < 0.005, ***p < 0.001, compared to the BLM group. $^{\#\#}$ p < 0.005, $^{\#\#\#}$ p < 0.001, compared to the Ctrl group.

we sought to clarify whether QM has pharmacological effects in regulating and improving endothelial injury and vascular remodeling, using zebrafish as an in vivo experimental model for further exploration. This study focused primarily on two aspects: efficacy in promoting vascular regeneration and efficacy in improving vascular endothery injury. Initially, the maximum tolerable concentration (MTC) method was employed to determine the appropriate QM dosage for zebrafish (Tables S8 and S9). The results indicated that in terms of vascular regeneration, the subintestinal vessel area in the zebrafish model group was significantly reduced compared to the normal control group. However, post-treatment with QM or Astragaloside IV, there was a notable increase in their vascular area expression (Figure 13A and B). Note: The yellow dashed frame indicates the analyzed subintestinal vessels. Regarding improvement in endothelial injury, the diameter of the intersegmental blood vessels in the model group of zebrafish was notably reduced relative to the normal control group. Post-treatment with QM or Aspirin, this diameter was effectively restored (Figure 13C and D). Note: The yellow dashed frame indicates the analyzed three intersegmental blood vessels above the zebrafish cloacal pore. Additionally, it was observed that treatment with QM or Aspirin significantly lowered the incidence of thrombosis in zebrafish compared to the model group (Figure 13E and F). Note: The yellow arrow indicates thrombosis. When assessing changes in blood flow velocity and cardiac output among different zebrafish groups, a significant decrease in these parameters was found in the model group compared to the normal control. Conversely, in zebrafish treated with QM or Aspirin, there was a significant increase in both blood flow velocity and cardiac output (Figure 13G and H). These findings conclusively demonstrate that QM treatment can significantly foster vascular regeneration and provide protective effects against vascular endothelial cell damage, underscoring its potential therapeutic value in vascular-related disorders.

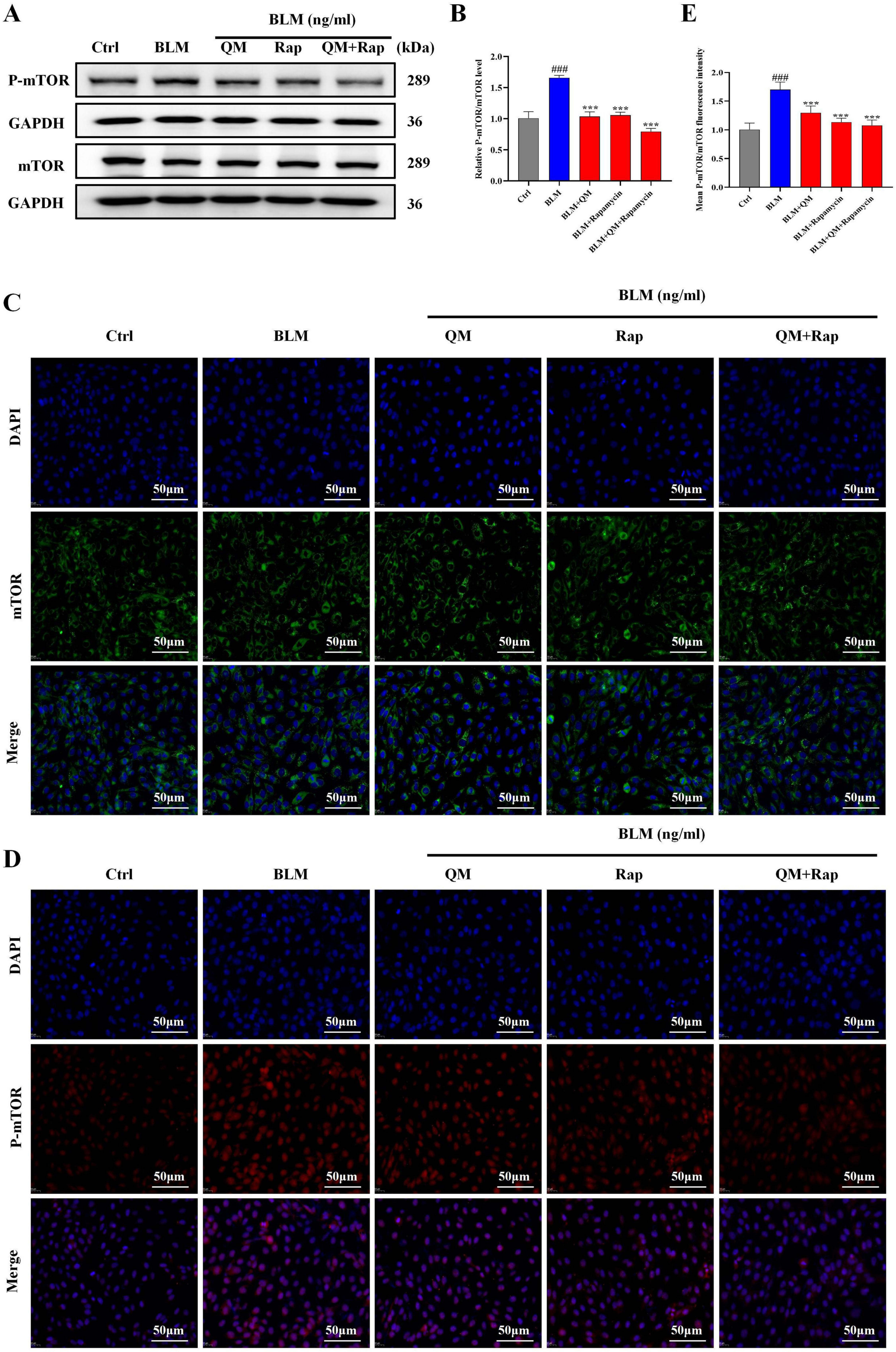

Figure 9 Verification of QM inhibiting the overexpression of P-mTOR: WB and IF methods after adding rapamycin. (**A**) WB detection of P-mTOR and mTOR protein expressions. (**B**) Quantitative analysis of protein expressions using Image J software. (**C** and **D**) Representative IF images of mTOR and P-mTOR. (Scale bar = 50 μm). (**E**) Quantitative analysis of positive expression of P-mTOR/mTOR protein (n = 3). ***$p < 0.001$, compared to the BLM group. $^{\#\#\#}$ $p < 0.001$, compared to the Ctrl group.

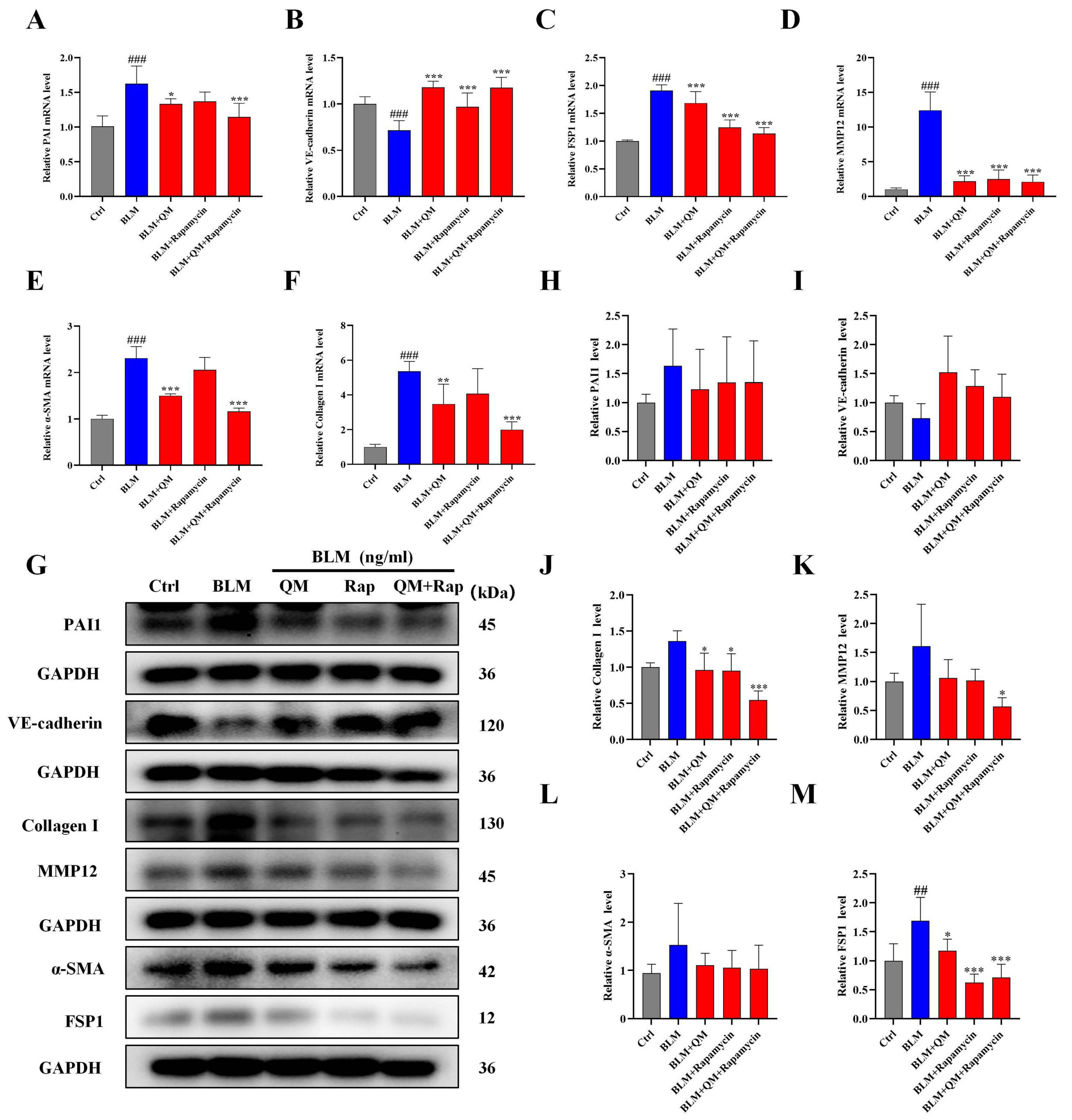

Figure 10 Evaluation of autophagy activator's (rapamycin) effect on EndMT in HUVECs via qPCR and WB. (**A**–**F**) qPCR analysis for mRNA expression levels of PAI, VE-cadherin, FSP1, MMP12, α-SMA, and Collagen I in HUVECs. (**G**) WB investigation of these proteins' expression in HUVECs. (**H**-**M**) Image J software quantification of protein expression (n ≥ 3). * $p < 0.05$, ** $p < 0.005$, *** $p < 0.001$, compared to the BLM group. $^{\#\#}$ $p < 0.005$, $^{\#\#\#}$ $p < 0.001$, compared to the Ctrl group.

Discussion

QM is a TCM prescription that has been demonstrated to prevent PF through our previous studies.[27] However, its pharmacological mechanisms require further elucidation. After screening, we identified 10 active ingredients with targets from QM-treated mouse plasma and lung tissues. These ingredients, including 3′,4′,7-trihydroxyisoflavone, 3-indoleacrylic acid, daidzein, isoliquiritigenin, licoricesaponin a3, liquiritin, neoisoliquiritin, ononin, and schaftoside, are considered important compounds in QM. The therapeutic potential of natural TCM has attracted significant attention from people. Famous researchers around the world have recognized the substantial benefits of natural TCM and its components in treating respiratory diseases. For example,

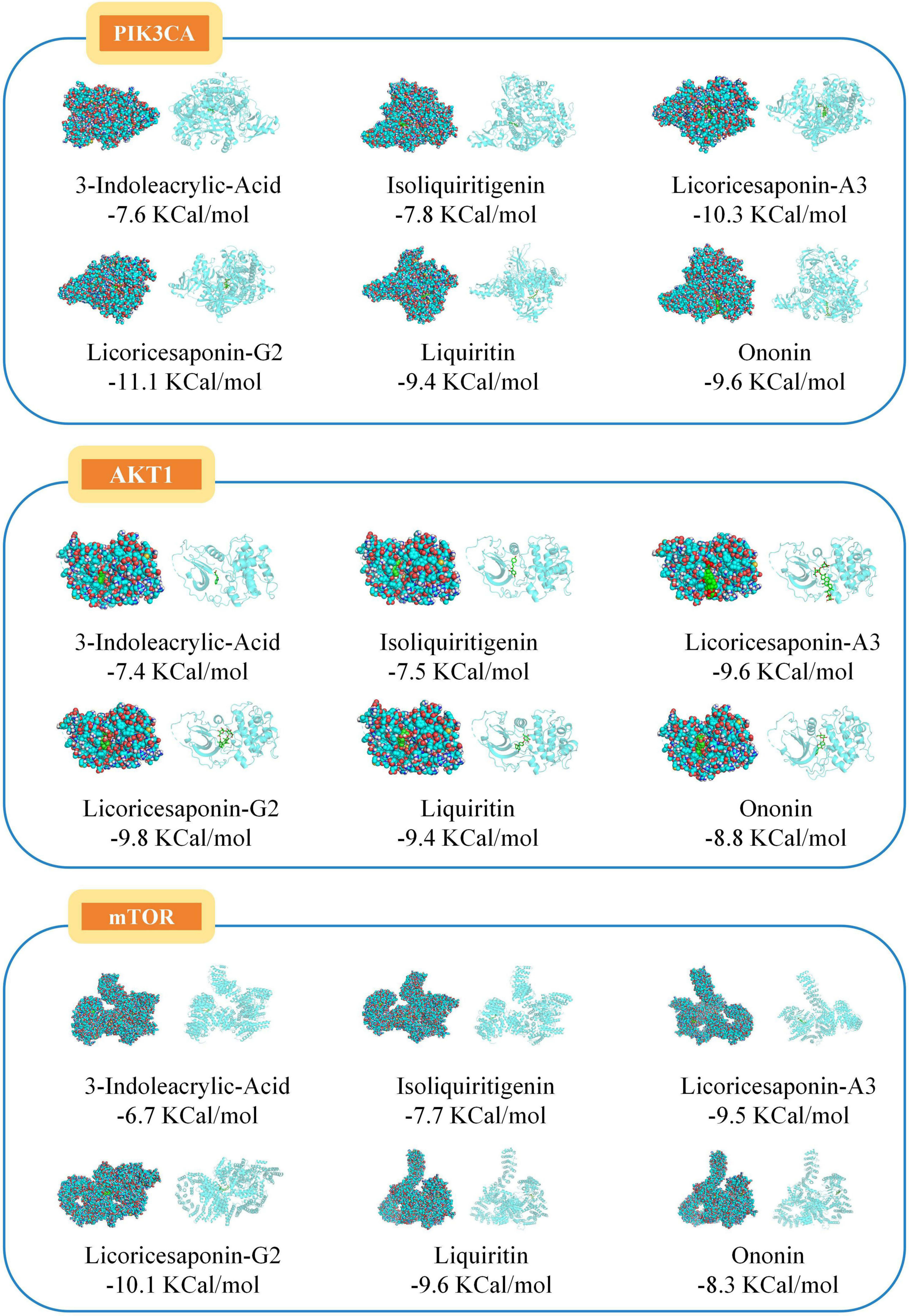

Figure 11 Molecular docking analysis. Molecular docking showed that drug-active compounds bind to PIK3CA, AKT1, and mTOR.

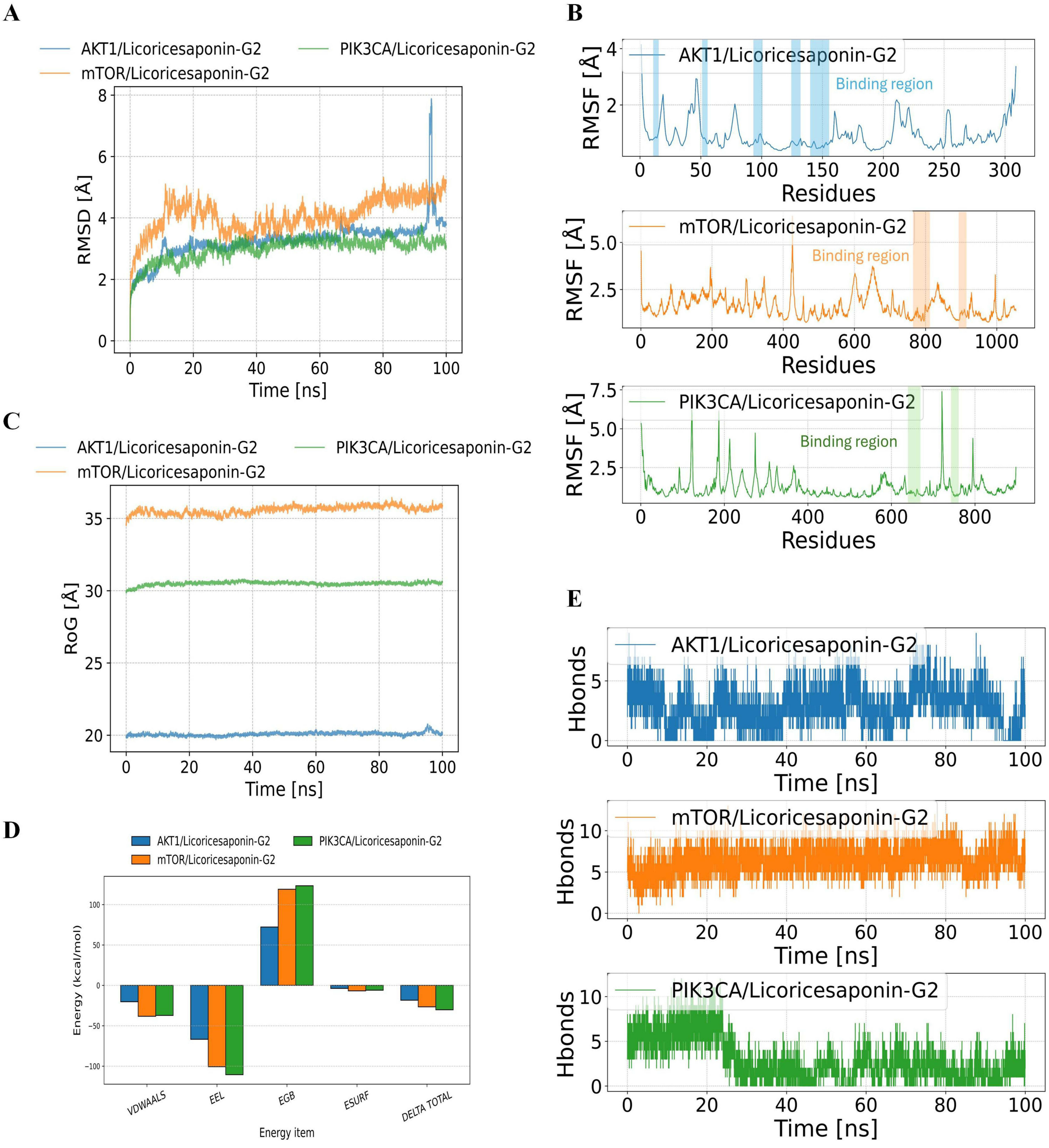

Figure 12 Molecular dynamics simulation results. (**A**) Ligand RMSD variations of three protein-Licoricesaponin-G2 complexes during 100 ns simulation. (**B**) Protein RMSF analysis of the three complexes. (**C**) Radius of gyration (RoG) changes over simulation time. (**D**) MM-GBSA binding energies and energy decomposition. (**E**) Number of hydrogen bonds between small molecule and proteins during MD simulation.

isoliquiritigenin significantly alleviated lipopolysaccharide (LPS)-induced acute lung injury (ALI) in mice, and the mechanisms underlying this preventive effect might include the alleviation of oxidative injury and inflammatory damage.[44] Similarly, liquiritin exerted protective effects against LPS-induced ALI by suppressing the activation of JNK and inhibiting the Nur77/c-Jun signaling pathway both in vivo and in vitro.[45] Isorhamnetin, a flavonol aglycone isolated from the plant Hippophae rhamnoides L, can attenuate BLM-induced EMT and PF and suppress BLM-induced ERS and the activation of PERK signaling.[46] Therefore, the multi-component, multi-target, and multi-pathway approach of natural TCM has become

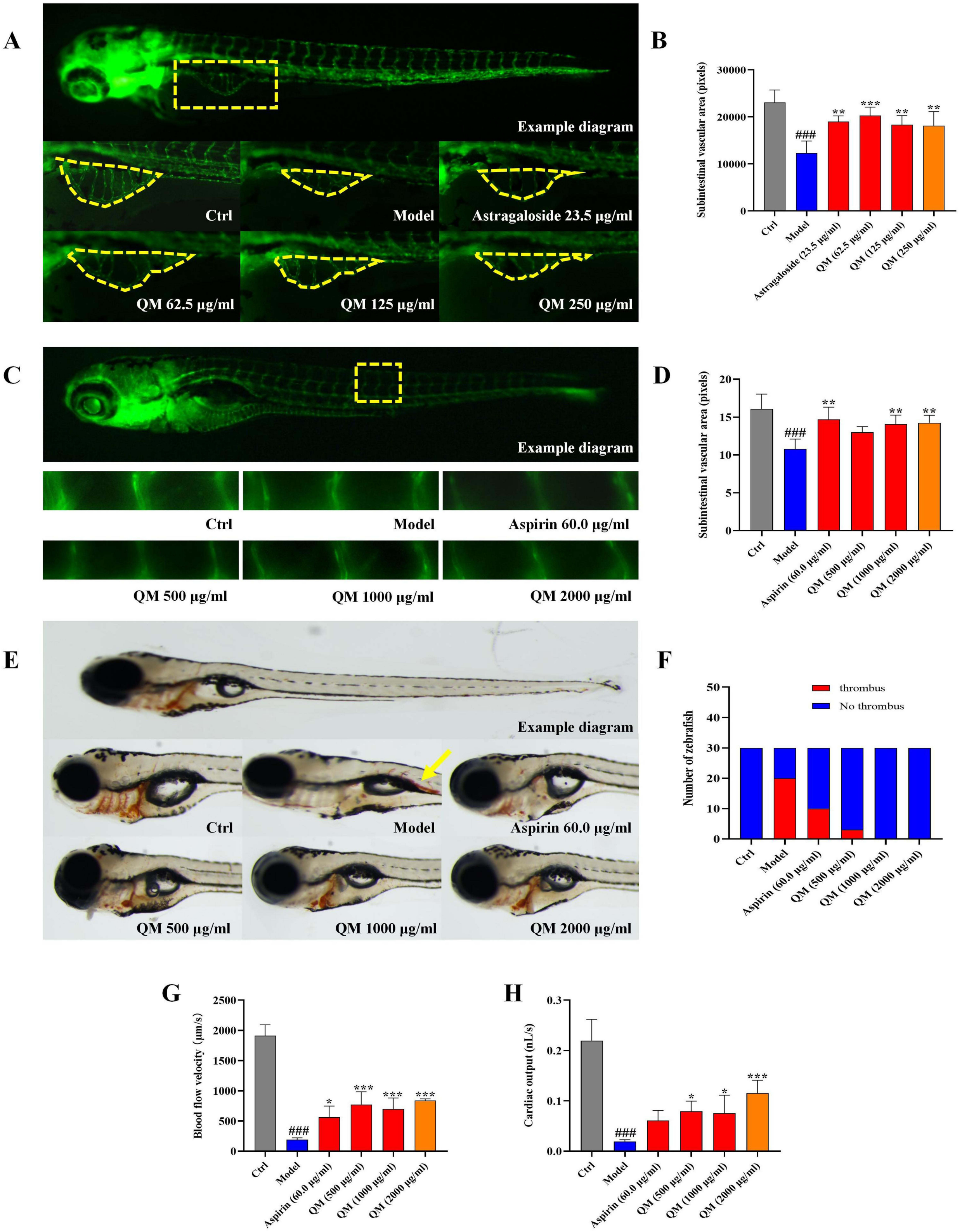

Figure 13 Zebrafish model validation of QM's efficacy in vascular regeneration and endothelial repair. (**A**) Typical image of the subintestinal vessel area in zebrafish after QM treatment. Note: (Yellow dashed box: the analyzed subintestinal vessel area). (**B**) Quantitative measurement of the expression of subintestinal vessel area in zebrafish. (**C**) Typical image of the intersegmental vessel diameter in zebrafish after QM treatment. (Yellow dashed box: the three intersegmental vessels above the zebrafish's cloacal pore). (**D**) Quantitative measurement of the expression of intersegmental vessel diameter in zebrafish. (**E**) Typical image of thrombosis in zebrafish (Yellow arrow: thrombosis). (**F**) Quantitative measurement of thrombosis occurrence in zebrafish. (**G**) Blood flow velocity in zebrafish after QM treatment. (**H**) Cardiac output in zebrafish after QM treatment. (n = 5). $^{*}p < 0.05$, $^{**}p < 0.005$, $^{***}p < 0.001$, compared to the Model group. $^{\#\#\#}$ $p < 0.001$, compared to the Ctrl group.

a distinctive feature in pharmaceutical research. Accordingly, the beneficial effects of QM in the treatment of PF may be attributed to the composition of these core compounds. Further experiments are necessary to supplement and verify the pharmacological properties of these relevant compounds. Building on the identified components, we can predict the potential mechanisms of QM in preventing PF more accurately through network pharmacology. Subsequently, 293 active compound targets and 1289 PF disease targets were retrieved through multiple databases, and 80 overlapping targets between QM and PF were identified. Using the visualization software Cytoscape, we constructed the compound-disease target network. Based on the STRING database, a PPI network was developed through these 80 overlapping targets, identifying key targets of QM against PF, including IL6, AKT1, MMP9, and TP53. IL-6, the protein node with the highest centrality in the core PPI network, is a critical pro-inflammatory cytokine that plays a crucial role in the PF process, influencing endothelial dysfunction, macrophage polarization, inflammation, and immunity.[47] AKT1, as a central node in the PI3K/AKT signaling pathway, could participate in PF by regulating downstream pathways such as mTOR and ROS.[48] Given that PF is characterized by abnormal remodeling of the ECM. MMP9, the principal enzyme that degrades type IV collagen, is shown to play a crucial role in regulating the ECM balance during PF.[49] TP53, a tumor suppressor gene, is pivotal in processes like cell cycle control, apoptosis, tumor development, and malignant transformation, and has been confirmed to significantly influence the regulation of PF.[50] The above results indicate that the core genes IL-6, AKT1, MMP9, and TP53 may be potential targets for exploring the treatment of PF from multiple perspectives, including inflammation, oxidative stress, endothelial injury, and autophagy.

GO and KEGG pathway enrichment analyses identified key pathways such as the “AGE-RAGE signaling pathway”, “PI3K-AKT signaling pathway”, and the “TNF signaling pathway” as critical in inhibiting the progression of PF. AGEs are formed through non-enzymatic reactions of lipids and proteins with various oxidants during aging. The receptors for AGEs have established a link between the process of PF and alveolar homeostasis. Moreover, previous studies have indicated an imbalance of AGEs/RAGEs during the progression of PF.[51] The PI3K/AKT signaling pathway plays a pivotal role in epithelial cell damage, immune activation, and fibroblast accumulation, and it is also involved in PF by targeting downstream proteins such as mTOR, HIF-1 alpha, and the FOX family.[52] TNF-α, a cytotoxic cytokine, has been shown to drive PF by activating the NF-κB signaling pathway.[53] Overall, the findings from network pharmacology suggest that QM may alleviate PF by inhibiting endothelial cell injury, primarily through reducing PI3K/AKT pathway-mediated restoration of autophagy. However, other related potential targets and signaling pathways have not been exhaustively covered in this study and warrant further investigation through supplementary experiments.

ECs are essential in forming a barrier between blood and tissues, playing a pivotal role in regulating permeability, resolving inflammation, balancing coagulation, and promoting angiogenesis.[54] These cells, which are in direct contact with blood, are crucial for maintaining vascular homeostasis and ensuring vascular integrity under normal physiological conditions.[55] However, external stimuli can trigger endothelial cell activation, leading to disruptions in vascular integrity. Such activation may result in vascular relaxation, reduced angiogenesis, loss of specific endothelial markers, secretion of pro-fibrotic mediators, and acquisition of mesenchymal-like features, causing significant alterations in gene expression, morphology, and function of the cells.[56] ECs dysfunction is closely associated with various diseases. For instance, in db/db mice and high glucose-induced Glomerular Endothelial Cells (GEnCs), Rutin has been shown to inhibit HDAC3 expression via the PI3K/AKT/mTOR pathway, restore autophagy, and reduce EndMT, suggesting its potential as a therapy for diabetic kidney disease (DKD) progression.[57] The activation of the osteopontin/CD44 axis, which induces EndMT, has been implicated in neointimal hyperplasia in dysfunctional arteriovenous fistulas, identifying a potential therapeutic target.[58] Single-cell sequencing of 15 cardiomyopathy (CM) patients revealed that among 112,670 cells, ECs constituted about 8%, followed by mural cells, highlighting the importance of ECs, EndMT, and mural cells in CM pathogenesis and offering novel insights into gene expression changes in CMs.[59] In line with our hypothesis, mice modeled with BLM exhibited clear PF symptoms in Micro CT scans, including high-density shadows, disordered lung texture, bronchial dilation, and vascular thickening. After two weeks of gavage treatment with QM, a significant reduction in PF symptoms was observed. Histological analyses, including H&E and Masson’s trichrome staining, showed that QM treatment effectively reduced inflammation and collagen fiber deposition in mouse lung tissue. At the molecular level, in BLM-induced C57 mice and HUVECs, QM treatment decreased the over-expression of mesenchymal markers (FSP1, MMP12, Collagen I, α-SMA, PAI1) and reinstated endothelial characteristics (VE-cadherin), supporting its potential as a therapeutic agent in the management of PF.

https://doi.org/10.2147/JIR.S515286

Research has established that EndMT critically disrupts vascular homeostasis, leading to vascular remodeling. This remodeling process typically involves inflammatory cell infiltration near blood vessels, thickening and narrowing of the vascular intima, and potentially, vascular occlusion.[60] Our study confirms the anti-EndMT effects of QM; however, its ability to maintain vascular homeostasis and improve hemodynamic functions required further investigation. Zebrafish embryos, known for their external development and transparent anatomy, serve as ideal models for studying vascular development.[61] Utilizing this model for empirical validation, our research found that QM treatment significantly increased the area of subintestinal vessels and the diameter of intersegmental blood vessels in zebrafish, surpassing the control model's results. Additionally, it effectively prevented thrombosis while enhancing blood flow velocity and cardiac output. In summary, our studies employing BLM-induced C57 mice and HUVECs models have successfully illustrated the anti-EndMT capabilities of QM. Supported by findings from the zebrafish model, these results further underscore QM's efficacy in promoting vascular regeneration and protecting against endothelial damage. Key benefits of QM include improvement in the architecture of intersegmental vessels, enhancement of hemodynamics, and prevention of thrombosis, demonstrating its potential as a therapeutic agent in vascular health management.

Autophagy is a complex, lysosome-dependent metabolic system crucial for degradation, regulated by autophagy-related genes and protein complexes.[62] It plays a vital role in maintaining cellular homeostasis by eliminating accumulated proteins, dysfunctional organelles, lipid deposits, and invasive pathogens.[63] Serving as a self-defense mechanism, autophagy is integral to the progression of a range of diseases, including neurodegenerative,[64] digestive system diseases,[65] cancer,[66] skeletal muscle disorders,[67] cardiovascular,[68] and respiratory diseases.[69] Disruption in EC homeostasis is a key precursor to many diseases, with EndMT being a critical process in this disruption. The potential of autophagy in regulating disease progression via EndMT has gained considerable interest in recent research. For instance, in the TAC rat model, Gentiana acuta was found to inhibit the PI3K/AKT/FoxO1/3a and Notch signaling pathways, mitigating myocardial fibrosis, hypertrophy, and autophagy, ultimately blocking EndMT and providing cardiac protection.[70] Additionally, studies indicate that autophagy defects in ECs can trigger IL6 synthesis/secretion, leading to EndMT and tissue fibrosis, suggesting that targeting ECs autophagy defects could be a viable therapeutic approach for vascular and metabolic diseases.[71] In our study with BLM-induced C57 mice and HUVECs, various methods were employed to assess the expression of autophagy-related proteins (Beclin-1 and LC3B). Following BLM treatment, a notable inhibition in the expression of these autophagy proteins was observed, while treatment with QM significantly restored their levels. Consequently, our findings suggest that QM can alleviate EndMT by reinstating autophagy processes.

The PI3K signaling pathway is widely recognized for its role in various diseases, a central regulator of autophagy, is crucial in both initiating and controlling this cellular process.[72] This pathway is increasingly seen as a vital target in drug development and disease treatment strategies. For instance, a major component of Danshen, Tanshinone I, has demonstrated potential as an anticancer agent, particularly for ovarian cancer. It has been reported to induce apoptosis through Caspase-3 cleavage and attenuate autophagy by inhibiting the activation of the PI3K/AKT/mTOR pathway.[73] Similarly, in rat models of myocardial ischemia/reperfusion injury (MIRI) and H9C2 cells, ginsenoside Rb1 has been found to activate the PI3K/AKT/mTOR pathway, reduce cardiomyocyte autophagy, and alleviate MIRI, as well as protect H9C2 cells from hypoxia/reoxygenation damage.[74] Our research corroborates these findings, demonstrating that QM significantly inhibits phosphorylation within this pathway in both in vivo and in vitro models, confirming its role as an upstream autophagy regulator. mTOR, activated and phosphorylated by AKT, plays a critical role in regulating cell survival and function across a variety of cell types by inhibiting autophagy.[75] As such, mTOR is a key pharmacological target in autophagy research. Rapamycin, a selective inhibitor of the mTOR kinase, has been extensively used in clinical applications for treating related diseases.[76] Our study enhances this understanding by showing that the addition of rapamycin reduces the overexpression of phosphorylated mTOR in HUVECs, with a more pronounced effect observed when QM is combined with rapamycin. These findings confirm the involvement of the PI3K/AKT/mTOR pathway in autophagy-mediated EndMT. Furthermore, based on molecular docking and molecular dynamics simulation, we confirmed that the active ingredients have good binding affinity with PIK3CA, AKT1, and mTOR, indicating that QM regulates PF disease progression through the PI3K/AKT/mTOR signaling pathway.

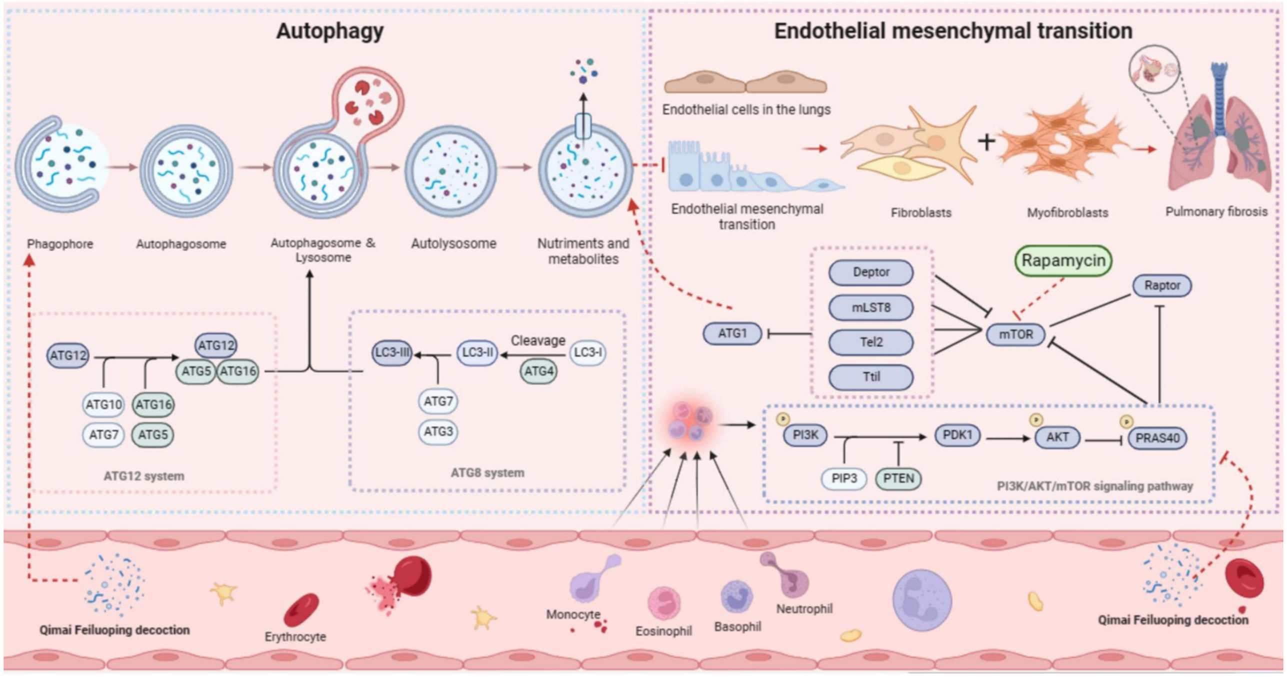

Figure 14 QM's mechanism in pulmonary fibrosis: restoring autophagy and inhibiting PI3K/AKT/mTOR to alleviate EndMT.

Conclusion

In both BLM-induced C57 mice and HUVECs, along with zebrafish, QM was found to alleviate EndMT by restoring autophagy, primarily through inhibition of the PI3K/AKT/mTOR signaling pathway, also could improve a range of vascular functional disorders and remodeling issues following EndMT (Figure 14). The present findings provide theoretical insight and delineate a previously unrecognized molecular pathway for PF therapy. Further in-vivo and in-vitro investigations are required to confirm QM's antifibrotic efficacy, identify additional targets and signaling cascades, and broaden the experimental evidence base for this formulation.

Abbreviations

PF, pulmonary fibrosis; EndMT, endothelial mesenchymal transition; QM, Qimai Feiluoping decoction; BLM, bleomycin; HUVECs, human umbilical vein endothelial cells; WB, Western blot; qPCR, quantitative Real-Time PCR; IHC, immunohistochemistry; IF, immunofluorescence; TEM, transmission electron microscopy; IPF, idiopathic pulmonary fibrosis; COVID-19, coronavirus disease 2019; PFD, pirfenidone; ECs, endothelial cells; ARDS, acute respiratory distress syndrome; ROS, reactive oxygen species; PMS, plantamajoside; AGEs, advanced glycation end products; CHF, congestive heart failure; HPMECs, human pulmonary microvascular endothelial cells; TCM, traditional Chinese medicine; RCT, randomized controlled clinical trial; CT, computed tomography; H&E, Hematoxylin & Eosin; EMT, epithelial mesenchymal transition; ECM, extracellular matrix; UHPLC/IM-QTOF-MS, UPLC I-Class/Vion IMS-QTOF system; PPI, protein-protein interaction; BC, Betweenness centrality; CC, Closeness centrality; DC, Degree centrality; CC, Cellular components; MF, molecular function; BP, biological processes; GO, gene ontology; KEGG, Kyoto encyclopedia of genes and genomes; PDB, protein data bank; PE, phosphatidylethanolamine; M, mitochondria; RER, rough endoplasmic reticulum; ASS, autophagic lysosomes; MTC, maximum tolerable concentration; LPS, lipopolysaccharide; GEnCs, Glomerular Endothelial Cells; ALI, acute lung injury; DKD, diabetic kidney disease; CM, cardiomyopathy; MIRI, myocardial ischemia/reperfusion.

Data Sharing Statement

The original contributions presented in the study are included in the article/supplementary material, further inquiries can be directed to the corresponding authors.

Ethics Statement

The research is exempt from ethical approval under items 1 and 2 of Article 32 of the Measures for Ethical Review of Life Science and Medical Research Involving Human Subjects dated February 18, 2023, China.

The animal study was approved by the experimental protocol involving animals was approved by the Experimental Animal Ethics Committee of Changchun University of Chinese Medicine (Approval No. 2023589). The study was conducted in accordance with the local legislation and institutional requirements.

Acknowledgments

The Northeast Asia Institute of Traditional Chinese Medicine, Changchun University of Chinese Medicine has provided excellent technical support.

Author Contributions

All authors contributed to data analysis, drafting or revising the article, have agreed on the journal to which the article will be submitted, gave final approval of the version to be published, and agree to be accountable for all aspects of the work.

Funding

This work was supported by Special Project for Emergency of the Ministry of Science and Technology, China (No.2020YFC0845000), Project of Jilin Province Science and Technology Development (No.YDZJ202501ZYTS697) and Project of Jilin Administration of Traditional Chinese Medicine, China (No.2022221).

Disclosure

The authors report no conflicts of interest in this work.

References

1. Lederer DJ, Martinez FJ. Idiopathic pulmonary fibrosis. *N Engl J Med*. 2018;378(19):1811–1823. doi:10.1056/NEJMra1705751
2. Sgalla G, Kulkarni T, Antin-Ozerkis D, et al. Update in pulmonary fibrosis 2018. *Am J Respir Crit Care Med*. 2019;200(3):292–300. doi:10.1164/rccm.201903-0542UP
3. Moss BJ, Ryter SW, Rosas IO. Pathogenic mechanisms underlying idiopathic pulmonary fibrosis. *Annu Rev Pathol*. 2022;17:515–546. doi:10.1146/annurev-pathol-042320-030240
4. Chambers RC, Mercer PF. Mechanisms of alveolar epithelial injury, repair, and fibrosis. *Ann Am Thorac Soc*. 2015;12(Suppl 1):S16–20. doi:10.1513/AnnalsATS.201410-448MG
5. Chanda D, Otoupalova E, Smith SR, et al. Developmental pathways in the pathogenesis of lung fibrosis. *Mol Aspects Med*. 2019;65:56–69. doi:10.1016/j.mam.2018.08.004
6. King TE Jr, Pardo A, Selman M. Idiopathic pulmonary fibrosis. *Lancet*. 2011;378(9807):1949–1961. doi:10.1016/S0140-6736(11)60052-4
7. Moon SW, Kim SY, Chung MP, et al. Longitudinal changes in clinical features, management, and outcomes of idiopathic pulmonary fibrosis. a nationwide cohort study. *Ann Am Thorac Soc*. 2021;18(5):780–787. doi:10.1513/AnnalsATS.202005-451OC
8. Maher TM, Bendstrup E, Dron L, et al. Global incidence and prevalence of idiopathic pulmonary fibrosis. *Respir Res*. 2021;22(1):197. doi:10.1186/s12931-021-01791-z
9. George PM, Wells AU, Jenkins RG. Pulmonary fibrosis and COVID-19: the potential role for antifibrotic therapy. *Lancet Respir Med*. 2020;8(8):807–815. doi:10.1016/S2213-2600(20)30225-3
10. Huang C, Huang L, Wang Y, et al. 6-month consequences of COVID-19 in patients discharged from hospital: a cohort study. *Lancet*. 2023;401(10393):e21–e33. doi:10.1016/S0140-6736(23)00810-3
11. King TE Jr, Bradford WZ, Castro-Bernardini S, et al. A Phase 3 trial of pirfenidone in patients with idiopathic pulmonary fibrosis. *N Engl J Med*. 2014;370(22):2083–2092. doi:10.1056/NEJMoa1402582
12. Flaherty KR, Wells AU, Cottin V, et al. Nintedanib in progressive fibrosing interstitial lung diseases. *N Engl J Med*. 2019;381(18):1718–1727. doi:10.1056/NEJMoa1908681
13. Maher TM, Corte TJ, Fischer A, et al. Pirfenidone in patients with unclassifiable progressive fibrosing interstitial lung disease: a double-blind, randomised, placebo-controlled, Phase 2 trial. *Lancet Respir Med*. 2020;8(2):147–157. doi:10.1016/S2213-2600(19)30341-8
14. Habermann AC, Gutierrez AJ, Bui LT, et al. Single-cell RNA sequencing reveals profibrotic roles of distinct epithelial and mesenchymal lineages in pulmonary fibrosis. *Sci Adv*. 2020;6(28):eaba1972. doi:10.1126/sciadv.aba1972
15. Dugina VB, Shagieva GS, Shakhov AS, et al. The Cytoplasmic Actins in the Regulation of Endothelial Cell Function. *Int J Mol Sci*. 2021;22(15):7836. doi:10.3390/ijms22157836
16. Kovacic JC, Dimmeler S, Harvey RP, et al. Endothelial to mesenchymal transition in cardiovascular disease: JACC state-of-the-art review. *J Am Coll Cardiol*. 2019;73(2):190–209. doi:10.1016/j.jacc.2018.09.089
17. Hou J, Shi J, Chen L, et al. M2 macrophages promote myofibroblast differentiation of LR-MSCs and are associated with pulmonary fibrogenesis. *Cell Commun Signal*. 2018;16(1):89. doi:10.1186/s12964-018-0300-8

18. Turner-Warwick M. Precapillary Systemic-pulmonary Anastomoses. *Thorax*. 1963;18(3):225–237. doi:10.1136/thx.18.3.225
19. Zhang R, Tan Y, Yong C, et al. Pirfenidone ameliorates early pulmonary fibrosis in LPS-induced acute respiratory distress syndrome by inhibiting endothelial-to-mesenchymal transition via the Hedgehog signaling pathway. *Int Immunopharmacol*. 2022;109:108805. doi:10.1016/j.intimp.2022.108805
20. Zhao W, Wang L, Yang J, et al. Endothelial cell-derived MMP19 promotes pulmonary fibrosis by inducing E(nd)MT and monocyte infiltration. *Cell Commun Signal*. 2023;21(1):56. doi:10.1186/s12964-023-01040-4
21. Folkerts H, Hilgendorf S, Vellenga E, et al. The multifaceted role of autophagy in cancer and the microenvironment. *Med Res Rev*. 2019;39(2):517–560. doi:10.1002/med.21531
22. Mizushima N, Komatsu M. Autophagy: renovation of cells and tissues. *Cell*. 2011;147(4):728–741. doi:10.1016/j.cell.2011.10.026
23. Buratta S, Tancini B, Sagini K, et al. Lysosomal exocytosis, exosome release and secretory autophagy: the autophagic- and endo-lysosomal systems go extracellular. *Int J Mol Sci*. 2020;21(7):2576. doi:10.3390/ijms21072576
24. Jiang X, Shao M, Liu X, et al. Reversible treatment of pressure overload-induced left ventricular hypertrophy through Drd5 nucleic acid delivery mediated by functional polyaminoglycoside. *Adv Sci*. 2021;8(5):2003706. doi:10.1002/advs.202003706
25. Pan JA, Zhang H, Lin H, et al. Irisin ameliorates doxorubicin-induced cardiac perivascular fibrosis through inhibiting endothelial-to-mesenchymal transition by regulating ROS accumulation and autophagy disorder in endothelial cells. *Redox Biol*. 2021;46:102120. doi:10.1016/j.redox.2021.102120
26. Zhang L, Guo YN, Liu J, et al. Plantamajoside attenuates cardiac fibrosis via inhibiting AGEs activated-RAGE/autophagy/EndMT pathway. *Phytother Res*. 2023;37(3):834–847. doi:10.1002/ptr.7663
27. Yang Y, Ding L, Bao T, et al. Network pharmacology and experimental assessment to explore the pharmacological mechanism of qimai feiluoping decoction against pulmonary fibrosis. *Front Pharmacol*. 2021;12:770197. doi:10.3389/fphar.2021.770197
28. Ding L, Yang Y, Wang Z, et al. Qimai Feiluoping decoction inhibits mitochondrial complex I-mediated oxidative stress to ameliorate bleomycin-induced pulmonary fibrosis. *Phytomedicine*. 2023;112:154707. doi:10.1016/j.phymed.2023.154707
29. Szklarczyk D, Gable AL, Lyon D, et al. STRING v11: protein-protein association networks with increased coverage, supporting functional discovery in genome-wide experimental datasets. *Nucleic Acids Res*. 2019;47(D1):D607–D613. doi:10.1093/nar/gky1131
30. Lipinski CA, Lombardo F, Dominy BW, et al. Experimental and computational approaches to estimate solubility and permeability in drug discovery and development settings. *Adv Drug Deliv Rev*. 2001;46(1–3):3–26. doi:10.1016/S0169-409X(00)00129-0
31. Maier JA, Martinez C, Kasavajhala K, et al. ff14SB: improving the accuracy of protein side chain and backbone parameters from ff99SB. *J Chem Theory Comput*. 2015;11(8):3696–3713. doi:10.1021/acs.jctc.5b00255
32. Wang J, Wolf RM, Caldwell JW, et al. Development and testing of a general amber force field. *J Comput Chem*. 2004;25(9):1157–1174. doi:10.1002/jcc.20035
33. Sagui C, Darden TA. Molecular dynamics simulations of biomolecules: long-range electrostatic effects. *Annu Rev Biophys Biomol Struct*. 1999;28:155–179. doi:10.1146/annurev.biophys.28.1.155
34. Larini L, Mannella R, Leporini D. Langevin stabilization of molecular-dynamics simulations of polymers by means of quasisymplectic algorithms. *J Chem Phys*. 2007;126(10):104101. doi:10.1063/1.2464095
35. Genheden S, Ryde U. The MM/PBSA and MM/GBSA methods to estimate ligand-binding affinities. *Expert Opin Drug Discov*. 2015;10(5):449–461. doi:10.1517/17460441.2015.1032936
36. Chen Y, Zheng Y, Fong P, et al. The application of the MM/GBSA method in the binding pose prediction of FGFR inhibitors. *Phys Chem Chem Phys*. 2020;22(17):9656–9663. doi:10.1039/D0CP00831A
37. Nguyen H, Roe DR, Simmerling C. Improved generalized born solvent model parameters for protein simulations. *J Chem Theory Comput*. 2013;9(4):2020–2034. doi:10.1021/ct3010485
38. Lee TH, Yeh CF, Lee YT, et al. Fibroblast-enriched endoplasmic reticulum protein TXNDC5 promotes pulmonary fibrosis by augmenting TGFβ signaling through TGFBR1 stabilization. *Nat Commun*. 2020;11(1):4254. doi:10.1038/s41467-020-18047-x
39. Ding L, Li Y, Yang Y, et al. Wenfei Buqi Tongluo formula against bleomycin-induced pulmonary fibrosis by inhibiting TGF-β/Smad3 Pathway. *Front Pharmacol*. 2021;12:762998. doi:10.3389/fphar.2021.762998
40. Pedroza M, TT L, Lewis K, et al. STAT-3 contributes to pulmonary fibrosis through epithelial injury and fibroblast-myofibroblast differentiation. FASEB. *J*. 2016;30(1):129–140.
41. Zhang W, Chen G, Ren JG, et al. Bleomycin induces endothelial mesenchymal transition through activation of mTOR pathway: a possible mechanism contributing to the sclerotherapy of venous malformations. *Br J Pharmacol*. 2013;170(6):1210–1220.
42. Yao RQ, Ren C, Xia ZF, et al. Organelle-specific autophagy in inflammatory diseases: a potential therapeutic target underlying the quality control of multiple organelles. *Autophagy*. 2021;17(2):385–401. doi:10.1080/15548627.2020.1725377
43. Pei F, Ma L, Jing J, et al. Sensory nerve niche regulates mesenchymal stem cell homeostasis via FGF/mTOR/autophagy axis. *Nat Commun*. 2023;14(1):344. doi:10.1038/s41467-023-35977-4
44. Liu Q, Lv H, Wen Z, et al. Isoliquiritigenin activates nuclear factor Erythroid-2 related factor 2 to suppress the NOD-like receptor protein 3 inflammasome and inhibits the NF-κB pathway in macrophages and in acute lung injury. *Front Immunol*. 2017;8:1518. doi:10.3389/fimmu.2017.01518
45. Zhou H, Yang T, Lu Z, et al. Liquiritin exhibits anti-acute lung injury activities through suppressing the JNK/Nur77/c-Jun pathway. *Chin Med*. 2023;18(1):35. doi:10.1186/s13020-023-00739-3
46. Zheng Q, Tong M, Ou B, et al. Isorhamnetin protects against bleomycin-induced pulmonary fibrosis by inhibiting endoplasmic reticulum stress and epithelial-mesenchymal transition. *Int J Mol Med*. 2019;43(1):117–126. doi:10.3892/ijmm.2018.3965
47. Bian F, Lan YW, Zhao S, et al. Lung endothelial cells regulate pulmonary fibrosis through FOXF1/R-Ras signaling. *Nat Commun*. 2023;14(1):2560. doi:10.1038/s41467-023-38177-2
48. Larson-Casey JL, Deshane JS, Ryan AJ, et al. Macrophage Akt1 kinase-mediated mitophagy modulates apoptosis resistance and pulmonary fibrosis. *Immunity*. 2016;44(3):582–596. doi:10.1016/j.immuni.2016.01.001
49. Peng L, Wen L, Shi QF, et al. Scutellarin ameliorates pulmonary fibrosis through inhibiting NF-κB/NLRP3-mediated epithelial-mesenchymal transition and inflammation. *Cell Death Dis*. 2020;11(11):978. doi:10.1038/s41419-020-03178-2

50. Yang F, Du W, Tang Z, et al. Protective effects of Qing-Re-Huo-Xue formula on bleomycin-induced pulmonary fibrosis through the p53/IGFBP3 pathway. *Chin Med*. 2023;18(1):33. doi:10.1186/s13020-023-00730-y
51. Machahua C, Montes-Worboys A, Llatjos R, et al. Increased AGE-RAGE ratio in idiopathic pulmonary fibrosis. *Respir Res*. 2016;17(1):144. doi:10.1186/s12931-016-0460-2
52. Gong H, Lyu X, Liu Y, et al. Eupatilin inhibits pulmonary fibrosis by activating Sestrin2/PI3K/Akt/mTOR dependent autophagy pathway. *Life Sci*. 2023;334:122218. doi:10.1016/j.lfs.2023.122218
53. Jing F, Chen X, Xue J, et al. An herbal product alleviates bleomycin-induced pulmonary fibrosis in mice via regulating NF-κB/TNF-α signaling in macrophages. *Front Pharmacol*. 2022;13:805432. doi:10.3389/fphar.2022.805432
54. Dalal PJ, Muller WA, Sullivan DP. Endothelial cell calcium signaling during barrier function and inflammation. *Am J Pathol*. 2020;190(3):535–542. doi:10.1016/j.ajpath.2019.11.004
55. Zhou X, Zhang C, Yang S, et al. Macrophage-derived MMP12 promotes fibrosis through sustained damage to endothelial cells. *J Hazard Mater*. 2024;461:132733. doi:10.1016/j.jhazmat.2023.132733
56. Mao W, Fan Y, Wang X, et al. Phloretin ameliorates diabetes-induced endothelial injury through AMPK-dependent anti-EndMT pathway. *Pharmacol Res*. 2022;179:106205. doi:10.1016/j.phrs.2022.106205
57. Dong R, Zhang X, Liu Y, et al. Rutin alleviates EndMT by restoring autophagy through inhibiting HDAC1 via PI3K/AKT/mTOR pathway in diabetic kidney disease. *Phytomedicine*. 2023;112:154700. doi:10.1016/j.phymed.2023.154700
58. Chang CJ, Lai YJ, Tung YC, et al. Osteopontin mediation of disturbed flow-induced endothelial mesenchymal transition through CD44 is a novel mechanism of neointimal hyperplasia in arteriovenous fistulae for hemodialysis access. *Kidney Int*. 2023;103(4):702–718.
59. Ren J, Xiao X, Li R, et al. Single-cell sequencing reveals that endothelial cells, EndMT cells and mural cells contribute to the pathogenesis of cavernous malformations. *Exp Mol Med*. 2023;55(3):628–642. doi:10.1038/s12276-023-00962-w
60. Gorelova A, Berman M, Al Ghouleh I. Endothelial-to-Mesenchymal Transition in Pulmonary Arterial Hypertension. *Antioxid Redox Signal*. 2021;34(12):891–914. doi:10.1089/ars.2020.8169
61. Wen L, Yan W, Zhu L, et al. The role of blood flow in vessel remodeling and its regulatory mechanism during developmental angiogenesis. *Cell Mol Life Sci*. 2023;80(6):162. doi:10.1007/s00018-023-04801-z
62. Vargas JNS, Hamasaki M, Kawabata T, et al. The mechanisms and roles of selective autophagy in mammals. *Nat Rev Mol Cell Biol*. 2023;24(3):167–185. doi:10.1038/s41580-022-00542-2
63. Yamamoto H, Zhang S, Mizushima N. Autophagy genes in biology and disease. *Nat Rev Genet*. 2023;24(6):382–400. doi:10.1038/s41576-022-00562-w
64. Nechushtai L, Frenkel D, Pinkas-Kramarski R. Autophagy in parkinson's disease. *Biomolecules*. 2023;13(10):1435. doi:10.3390/biom13101435
65. Yang L, Ye F, Liu J, et al. Extracellular SQSTM1 exacerbates acute pancreatitis by activating autophagy-dependent ferroptosis. *Autophagy*. 2023;19(6):1733–1744. doi:10.1080/15548627.2022.2152209
66. Sun Y, Shen W, Hu S, et al. METTL3 promotes chemoresistance in small cell lung cancer by inducing mitophagy. *J Exp Clin Cancer Res*. 2023;42(1):65. doi:10.1186/s13046-023-02638-9
67. Liao S, Zheng Q, Shen H, et al. HECTD1-mediated ubiquitination and degradation of rubicon regulates autophagy and osteoarthritis pathogenesis. *Arthritis Rheumatol*. 2023;75(3):387–400. doi:10.1002/art.42369
68. Xing Y, Sui Z, Liu Y, et al. Blunting TRPML1 channels protects myocardial ischemia/reperfusion injury by restoring impaired cardiomyocyte autophagy. *Basic Res Cardiol*. 2022;117(1):20. doi:10.1007/s00395-022-00930-x
69. Zhang J, Wang H, Chen H, et al. ATF3 -activated accelerating effect of LINC00941/lncIAPF on fibroblast-to-myofibroblast differentiation by blocking autophagy depending on ELAVL1/HuR in pulmonary fibrosis. *Autophagy*. 2022;18(11):2636–2655. doi:10.1080/15548627.2022.2046448
70. Zhou WW, Dai C, Liu WZ, et al. Gentianella acuta improves TAC-induced cardiac remodelling by regulating the Notch and PI3K/Akt/FOXO1/3 pathways. *Biomed Pharmacother*. 2022;154:113564. doi:10.1016/j.biopha.2022.113564
71. Takagaki Y, Lee SM, Dongqing Z, et al. Endothelial autophagy deficiency induces IL6 - dependent endothelial mesenchymal transition and organ fibrosis. *Autophagy*. 2020;16(10):1905–1914. doi:10.1080/15548627.2020.1713641
72. Xu Z, Han X, Ou D, et al. Targeting PI3K/AKT/mTOR-mediated autophagy for tumor therapy. *Appl Microbiol Biotechnol*. 2020;104(2):575–587. doi:10.1007/s00253-019-10257-8
73. Zhou J, Jiang YY, Chen H, et al. Tanshinone I attenuates the malignant biological properties of ovarian cancer by inducing apoptosis and autophagy via the inactivation of PI3K/AKT/mTOR pathway. *Cell Proliferation*. 2020;53(2):e12739. doi:10.1111/cpr.12739
74. Qin GW, Lu P, Peng L, et al. Ginsenoside Rb1 inhibits cardiomyocyte autophagy via PI3K/Akt/mTOR signaling pathway and reduces myocardial ischemia/reperfusion injury. *Am J Chin Med*. 2021;49(8):1913–1927. doi:10.1142/S0192415X21500907
75. Chang Y, Deng H, He Y, et al. Wuzi Yanzong administration alleviates Sertoli cell injury by recovering AKT/mTOR-mediated autophagy and the mTORC1-mTROC2 balance in aging-induced testicular dysfunction. *J Ethnopharmacol*. 2024;318(Pt A):116865. doi:10.1016/j.jep.2023.116865
76. Chen Z, Guo Q, Huang S, et al. Overcoming adaptive resistance in AML by synergistically targeting FOXO3A-GNG7-mTOR axis with FOXO3A inhibitor Gardenoside and rapamycin. *Genes Dis*. 2024;11(1):397–412. doi:10.1016/j.gendis.2023.01.002